e-ISSN: 2687-6698 Research Article

Turkish Journal of

Analytical Chemistry

TurkJAC

https://dergipark.org.tr/tr/pub/turkjac

Advanced interpretation of kinetics and equilibrium data obtained from adsorption of Pb^{2+} ions from aqueous solution onto pine bark (*Pinus brutia* Ten.) using non-linear regression: A practical approach with Microsoft Excel Solver*

Ali Gundogdu[1], Volkan N. Bulut[2]**

[1] Karadeniz Technical University, Maçka Vocational School, Department of Pharmacy Services, 61750, Maçka, Trabzon, Türkiye
[2] Karadeniz Technical University, Maçka Vocational School, Department of Chemistry and Chemical Processing Technologies, 61750, Maçka, Trabzon, Türkiye

Abstract

This study investigates the adsorption of Pb^{2+} ions from aqueous solutions onto pine bark (*Pinus brutia* Ten.) using non-linear regression analysis to evaluate kinetic and equilibrium data. Adsorption experiments were conducted over a range of initial concentrations, and the equilibrium data were fitted to various two-parameter isotherm models, including Langmuir, Freundlich, Temkin, Dubinin-Radushkevich (D-R), and Jovanovic, as well as advanced three-parameter models like Dubinin -Astakhov (D-A), Tóth, Sips, Redlich-Peterson (R-P), and Brouers-Sotolongo (B-S). Kinetic data were analyzed using pseudo-first order (PFO), pseudo-second order (PSO), Elovich, Avrami, and Brouers-Sotolongo (B-S) models. Non-linear regression was performed using Microsoft Excel Solver, a readily accessible tool that eliminates the need for expensive software. Model parameters were optimized, and the goodness of fit was evaluated using multiple error functions, including SSE, ARE, HYBRID, MPSD, and MAE.

Results indicate that the Brouers-Sotolongo (B-S) model provided the best fit for both kinetic and isotherm data, reflecting the heterogeneous surface characteristics of the adsorbent. The adsorption process was found to involve a combination of physical and chemical interactions, as evidenced by the B-S kinetic constants (α_{BS} and n_{BS}) and the half-reaction time ($\tau_{1/2}$). Among the equilibrium models, three-parameter isotherms, particularly the B-S, Tóth, and Sips models, showed superior performance over two-parameter models, highlighting the complex nature of adsorption mechanisms in this system.

This study underscores the efficacy of pine bark as a low-cost and eco-friendly adsorbent for heavy metal removal and demonstrates the utility of non-linear regression and advanced error analysis in adsorption studies. This approach is thought to improve the precision of model selection and the understanding of adsorption mechanisms, contributing to the literature.

Keywords: Adsorption, error function, excel solver, isotherm, kinetics and equilibrium data, non-linear regression

1. Introduction

The process of adsorption is a cornerstone of environmental protection technologies, particularly for the removal of pollutants from aqueous environments. It is a versatile and efficient technique employed in wastewater treatment, heavy metal recovery, and the purification of drinking water. As the demand for cleaner water and more sustainable industrial practices grows, optimizing adsorption processes becomes increasingly important. The accurate interpretation of adsorption equilibrium and kinetic data is essential for designing efficient adsorbents and scaling up industrial applications. While traditional models provide foundational insights, recent advancements in computational techniques and error analysis have significantly enhanced the accuracy and predictive power of adsorption studies [1–3].

Adsorption equilibrium data, typically analyzed through isotherm models like Langmuir, Freundlich, Temkin, and Dubinin-Radushkevich, describe the relationship between the adsorbate concentration in the solution and the amount adsorbed onto the surface of the adsorbent. These models provide essential information

Citation: A. Gundogdu, V.N. Bulut, Advanced interpretation of kinetics and equilibrium data obtained from adsorption of Pb^{2+} ions from aqueous solution onto pine bark (*Pinus brutia* ten) using nonlinear regression: A Practical Approach with Microsoft Excel Solver, Turk J Anal Chem, 7(2), 2025, 108–131.

**Author of correspondence: a.ramazan.gundogdu@gmail.com
Tel: +90 (462) 512 3535 **Fax:** +90 (462) 512 3552

Received: January 25, 2025 **Accepted:** March 31, 2025

https://doi.org/10.51435/turkjac.1626570

*This paper was presented at the 6th International Environmental Chemistry Congress, EnviroChem 05-08 November 2024, Trabzon Türkiye.

about the adsorption capacity, surface heterogeneity, and the affinity of the adsorbate towards the adsorbent. However, the fitting of experimental data to these models can sometimes yield large deviations, especially when dealing with complex systems or heterogeneous adsorbents [4]. Researchers have therefore employed advanced techniques, including non-linear regression and error analysis, to enhance the reliability of adsorption isotherm model fitting. This is crucial because the accuracy of model predictions directly impacts the effectiveness of the adsorbent in real-world applications [4–6].

Non-linear regression, particularly when implemented through accessible tools like Microsoft Excel Solver, enables more precise fitting of data to isotherm models by minimizing the residuals (sum of squared errors). This approach reduces systematic bias often encountered with linearized versions of the models, where data transformations can distort the relationships between variables [7,8]. The use of error metrics such as the root mean square error (RMSE), coefficient of determination (R^2), and adjusted R^2 can further guide the selection of the most appropriate model, ensuring that it best describes the experimental data [9,10].

Adsorption kinetics studies the time-dependent behavior of adsorbate molecules on adsorbent surfaces. Traditional models, such as the pseudo-first order and pseudo-second order kinetic models, are commonly used to describe the rate of adsorption. However, these models often assume simple, linear adsorption mechanisms and do not always capture the complexities of real systems, where multiple factors (e.g., diffusion limitations, surface heterogeneity, chemical interactions) may influence the adsorption rate [11]. Recent studies have proposed hybrid kinetic models that combine multiple rate-limiting steps to better represent complex adsorption systems [12]. In these models, non-linear regression is again critical for fitting experimental data, as it provides a direct way to optimize parameters without introducing biases that can arise from linearization [13]. Non-linear regression methods, on the other hand, provide a more accurate and robust approach for fitting adsorption data, especially when dealing with complex adsorption behaviors [5].

Error analysis is particularly important when interpreting kinetic data. One key aspect is the propagation of error through model parameters. For example, when fitting experimental data to kinetic models, small measurement errors or uncertainties in the initial concentration of adsorbates can lead to significant discrepancies in the estimated rate constants [14]. To mitigate these issues, researchers often use methods such as bootstrapping or Monte Carlo simulations to assess the robustness of their kinetic models and quantify the uncertainty in parameter estimates. These approaches allow for a more comprehensive understanding of how errors in the experimental setup may influence the interpretation of adsorption dynamics [15].

While traditional methods of data analysis remain valuable, the increasing complexity of adsorption systems has driven the adoption of advanced computational tools. Non-linear regression, enabled by software like Microsoft Excel Solver, is one such tool that offers a more accessible and cost-effective alternative to more specialized programs like MATLAB, OriginPro, or Python. Solver works by adjusting the parameters of a predefined model to minimize the error between predicted and experimental data. This optimization approach eliminates the need for data transformations and offers a more direct way to assess model fit. Moreover, recent studies have shown that Solver, when combined with error analysis techniques, can achieve results that are comparable to those obtained with more advanced software packages, making it an attractive option for researchers in the field of adsorption [10,16].

In this study, the adsorption data of Pb^{2+} ions from aqueous solution onto pine bark (*Pinus brutia* Ten.) [17] were analyzed using non-linear regression models. The primary objective is to compare and interpret the kinetic and equilibrium data obtained from experiments by fitting them to widely used adsorption models, including pseudo-first order, pseudo-second order, Elovich, Avrami, and Brouers-Sotolongo (B-S) for kinetic analysis, and Langmuir, Freundlich, Temkin, Dubinin-Radushkevich (D-R), Jovanovic, Dubinin-Astakhov (D-A), Redlich-Peterson (R-P), Sips, Toth, and Brouers-Sotolongo (B-S) models for adsorption equilibrium. To evaluate the goodness of fit, several error functions were applied, including sum of squared errors (SSE), average relative error (ARE), hybrid fractional error (HYBRID), Marquardt's percent standard deviation (MPSD), and mean absolute error (MAE). The use of Microsoft Excel Solver for non-linear regression fitting is demonstrated, emphasizing its simplicity, accessibility, and cost-effectiveness, especially when compared to other more complex and expensive software options.

Through this study, the goal is not only to provide a comprehensive comparison of these adsorption models but also to address some of the inconsistencies and inaccuracies found in the literature regarding the application of adsorption models. A significant issue in the literature is the frequent misapplication and misinterpretation of mathematical models, which can lead to misleading conclusions. By employing non-linear regression and performing error analysis, this study aims to provide more accurate and reliable results, contributing to a better understanding of Pb^{2+} adsorption processes and advancing the knowledge in this area.

Another aim of this study is to facilitate data analysis by enabling the Solver add-in in the low-cost and readily available Microsoft Excel and to propose it as a strong alternative to expensive software used for this purpose.

2. Material and method

2.1. Materials used and calculations

The preparation and characterization of the adsorbent, pine bark (*Pinus brutia* Ten.), are detailed in the literature [17]. The chemicals, materials, apparatus, and solutions employed in the adsorption tests are also described in the same reference.

The Pb^{2+} concentrations adsorbed onto the pine bark (q_e or q_t, mg/g) were calculated using the equation in **Formula (1)**, based on the difference between the initial (C_o, mg/L) and residual (C_e, mg/L) Pb^{2+} concentrations in the solution.

$$q_e \text{ or } q_t = \frac{(C_o - C_e)\cdot V}{m} \quad (1)$$

Where q_e represents the amount of Pb^{2+} adsorbed per unit mass of adsorbent at equilibrium (mg/g), q_t denotes the amount of Pb^{2+} adsorbed per unit mass of adsorbent at a specific time (mg/g), V is the solution volume (L), and m is the mass of the adsorbent (g).

2.2. Statistical evaluation

Each adsorption test was performed at least three times, and the average values were used. Microsoft Office 365 Excel was employed for data analysis and error function evaluations, while the Excel Solver add-in was utilized for non-linear regression analyses.

3. Theory

In this study, Pb^{2+} adsorption onto pine bark was investigated through equilibrium and kinetic analyses using non-linear regression methods. For the kinetic evaluation, the mathematical equations of the pseudo-first order (PFO), pseudo-second order (PSO), Elovich, Avrami, and Brouers-Sotolongo (B-S) models were applied. The adsorption equilibrium was analyzed using the mathematical equations of isotherm models, including Langmuir, Freundlich, Temkin, Dubinin-Radushkevich (D-R), Jovanovic, Dubinin-Astakhov (D-A), Redlich-Peterson (R-P), Sips, Toth, and Brouers-Sotolongo (B-S).

3.1. Adsorption kinetics models

3.1.1. Pseudo-first order (PFO) kinetic model

PFO kinetic model, proposed by Lagergren (1898), describes the adsorption rate based on the assumption that the rate of change in adsorption capacity is proportional to the difference between the adsorption capacity at equilibrium and the amount of adsorbed solute at any given time [18].

The equation for this model is:

$$q_t = q_e(1 - e^{-k_1 t}) \quad (2)$$

where:

- q_t is the amount of solute adsorbed at time t (mg/g),
- q_e is the amount of solute adsorbed at equilibrium (mg/g),
- k_1 is the rate constant of the pseudo-first order kinetic (1/min).

3.1.2. Pseudo-second order (PSO) kinetic model

The PSO model, proposed by Ho (2006), assumes that the rate of adsorption is proportional to the square of the difference between the equilibrium adsorption capacity and the amount of solute adsorbed at any given time. This model is widely used for its accuracy in modeling the adsorption of pollutants in aqueous solutions [19].

The equation for this model is:

$$q_t = \frac{q_e^2 k_2 t}{q_e k_2 t + 1} \quad (3)$$

where k_2 is the rate constant of the pseudo-second order kinetic (g/mg·min).

This model often fits well with adsorption data from aqueous solutions, especially for systems where the adsorption process is dominated by chemisorption [19].

3.1.3. Elovich kinetic model

The Elovich adsorption kinetic model is an empirical rate equation that shows adsorption energy grows linearly with surface coverage. This model holds that adsorption occurs at specified places, adsorbed ions interact, and the adsorbate concentration remains constant. It is suitable for both gas adsorption and wastewater treatment [20].

The equation for this model is:

$$q_t = \frac{1}{\beta_E} ln(1 + \alpha_E \beta_E t) \quad (4)$$

where:

- α_E is the initial adsorption rate (mg/g·min),
- β_E is related to the adsorption capacity (g/mg),

3.1.4. Avrami kinetic model

The primary goal of the Avrami model is to understand the rate and mechanism of crystallization or reaction processes. The Avrami kinetic model is also widely used in the processes of pollutant removal from aqueous environments through adsorption. Adsorption refers to the transition of pollutants from the liquid phase to a solid adsorbent surface. This process typically exhibits kinetic characteristics similar to crystallization and other physical-chemical reactions, which is why the Avrami model is suitable for understanding the rate and mechanism of adsorption reactions [21–23].

The Avrami equation is:

$$q_t = q_e[1 - \exp(-k_A t^{n_A})] \quad (5)$$

where k_A is the rate constant, and n_A is the Avrami exponent, a parameter that determines the adsorption mechanism and geometry. The unit of the rate constant k_A depends on the time unit (t) used. $k_A \approx t^{-n_A}$

- n = 1: One-dimensional adsorption on the surface or edge.
- n = 2: Two-dimensional adsorption (e.g., on planar surfaces).
- n = 3: Three-dimensional adsorption (e.g., in porous structures).
- n = 4: Three-dimensional adsorption with continuous nucleation (e.g., continuous formation of new adsorption sites) [23].

3.1.5. Brouers-Sotolongo (B-S) kinetic model

This model goes beyond traditional first and second-order kinetic models by including a fractal time parameter and a fractional order parameter. It provides better data fitting and helps in understanding the nature of processes. This model is especially useful for better understanding complex reactions and adsorption processes.

The Brouers-Sotolongo (B-S) kinetic model is represented by the following equation:

$$q_{n,\alpha}(t) = q_e\left[1 - \left(1 + (n_{BS} - 1)\left(\frac{t}{\tau_C}\right)^{\alpha_{BS}}\right)^{\frac{-1}{(n_{BS}-1)}}\right] \quad (6)$$

Where $q_{n,\alpha}(t)$) is the amount of substance adsorbed at time (t). q_e is the equilibrium adsorption capacity. n_{BS} is the fractional order parameter. α_{BS} is the fractal time parameter, and τ_C is the characteristic time constant.

The parameter n_{BS} allows the model to interpolate between different kinetic orders, providing flexibility in describing various kinetic processes. The parameter α_{BS} accounts for the complexity and irregularity of the kinetic process over time. τ_C, this is a scaling factor that adjusts the time scale of the process.

The half-reaction time, denoted as $\tau_{1/2}$, represents the duration required to absorb half of the equilibrium amount. It is calculated using the following equation:

$$\left[1 + (n_{BS} - 1)\left(\frac{t}{\tau_C}\right)^{\alpha_{BS}}\right]^{\frac{-1}{(n_{BS}-1)}} = \frac{1}{2} \quad (7)$$

which gives

$$\tau_{1/2} = \tau_C\left[\frac{2^{(n_{BS}-1)} - 1}{n_{BS} - 1}\right]^{\frac{1}{\alpha}} \quad (8)$$

$\tau_{1/2}$ represents the half-life time, which is the time required for the quantity of the substance to reduce to half of its initial value.

The B-S model is particularly useful in describing complex adsorption processes and drug release kinetics, offering a more accurate fit to experimental data compared to traditional kinetic models [24–27].

3.2. Adsorption isotherm models

3.2.1. Two-parameter isotherms

3.2.1.1. Langmuir adsorption isotherm:

The Langmuir adsorption isotherm assumes that adsorption occurs on a homogeneous surface with a finite number of identical sites. Each site can hold only one molecule, and the adsorption process is reversible. It is one of the most commonly used models for describing monolayer adsorption [28,29].

The non-linear Langmuir equation is:

$$q_e = \frac{q_m K_L C_e}{1 + K_L C_e} \quad (9)$$

where:

- q_e is the amount adsorbed at equilibrium (mg/g),
- q_m is the maximum adsorption capacity (mg/g),
- K_L is the Langmuir constant related to adsorption enthalpy (L/mg),
- C_e is the equilibrium concentration of solute (mg/L).

3.2.1.2. Freundlich adsorption isotherm:

The Freundlich model is an empirical model that describes adsorption on heterogeneous surfaces. Unlike Langmuir, it does not assume uniform adsorption sites, adsorption is more favorable at lower concentrations, and Freundlich allows for multilayer adsorption. It is applicable to systems with a wide range of energy.

The non-linear equation is:

$$q_e = K_F C_e^{\frac{1}{n_F}} \quad (10)$$

where K_F is the Freundlich constant related to adsorption capacity (L/g), and $1/n_F$ is an empirical constant representing the intensity or heterogeneity of adsorption. If $(1/n_F)<1$, adsorption is favorable, and $(1/n_F)>1$, adsorption is less effective. This model is widely used in environmental chemistry for predicting the adsorption behavior of various solutes [4,30].

Linear adsorption ($n_F=1$): The adsorption follows a simple linear relationship, indicating no cooperative or competitive effects.

Chemical interaction ($n_F<1$): Adsorption involves strong chemical interactions between the adsorbate and the surface.

Physical interaction ($n_F>1$): The adsorption process is dominated by weaker physical forces, such as van der Waals interactions [4].

3.2.1.3. Temkin adsorption isotherm:

The Temkin adsorption isotherm considers the interactions between the adsorbent (surface) and the adsorbate (molecule). This isotherm assumes that the heat of adsorption decreases linearly with increasing coverage of the surface. It is particularly useful for describing adsorption processes at low to moderate concentrations [31]. The model takes into account the non-uniform energy distribution on the surface and performs particularly well in the medium concentration range.

The Temkin isotherm equation is expressed as:

$$q_e = \frac{RT}{b_M} ln(K_M C_e) \quad (11)$$

where R is the universal gas constant with a value of 8.314 J/(mol·K). T represents the temperature in Kelvin. b_M is the Temkin constant related to the heat of sorption, measured in J/mg, and K_M is the Temkin isotherm constant, measured in L/g [32].

3.2.1.4. Dubinin-Radushkevich (D-R) adsorption isotherm:

The D-R isotherm is used to describe adsorption on microporous materials and is often applied to study the adsorption of gases and small molecules. Unlike Langmuir, it does not assume monolayer adsorption. It is based on the potential energy distribution on the surface of the adsorbent [32].

The non-linear equation for the D-R model is:

$$q_e = q_m \exp(-K_{DR}\varepsilon^2) \quad (12)$$

$$\varepsilon = RTln\left(1 + \frac{1}{C_e}\right) \quad (13)$$

where:

- K_{DR} is a constant related to the adsorption energy (mol²/kJ²),
- ε is the Polanyi potential (kJ/mol),
- R is the universal gas constant,
- T is the temperature (K).

This model is particularly useful for describing the adsorption of small molecules on solid adsorbents, especially in low-concentration regimes [33].

3.2.1.5. Jovanovic adsorption isotherm:

The Jovanovic adsorption isotherm is an extension of the Langmuir model, focusing on monolayer adsorption without lateral interactions between adsorbed molecules. It considers mechanical contact between adsorbing and desorbing molecules, making it suitable for systems involving localized adsorption. The isotherm can describe both physical and chemical adsorption processes and transitions to Henry's Law at low concentrations [32].

Jovanovic's mathematical equation is:

$$q_e = q_m(1 - e^{-K_J C_e}) \quad (14)$$

where K_J is the Jovanovic constant in L/mg [34]. The mathematical equation of the Jovanovic isotherm model shows significant similarity to the equation of the pseudo-first order kinetic model (Eq. 2).

3.2.2. Three-parameter isotherms

3.2.2.1. Dubinin-Astakhov (D-A) adsorption isotherm:

The D-A adsorption isotherm is a widely used model for describing adsorption in microporous materials, such as activated carbon and zeolites. It is an extension of the D-R isotherm, incorporating energy heterogeneity of the adsorbent surface. This model is commonly applied to describe the adsorption of organic or inorganic compounds from aqueous solutions [35].

The isotherm is mathematically expressed as:

$$q_e = q_m \exp\left[-\left(\frac{\varepsilon}{\sqrt{2E}}\right)^{n_{DA}}\right] \quad (15)$$

Where Ɛ is the Polanyi potential in kJ/mol (see Eq. (13)), as in the D-R equation. E is the characteristic adsorption energy (kJ/mol), indicating the energy barrier of the adsorption process, and n_{DA} is the exponent reflecting the heterogeneity of the adsorbent surface [36].

In the D-A adsorption isotherm, the n_{DA} parameter is known as a heterogeneity factor that expresses the surface heterogeneity of the adsorbent. This parameter reflects the homogeneity or heterogeneity of the pore distribution on the surface where adsorption occurs. The n_{DA} value indicates how diverse the pore sizes on the surface are; higher n_{DA} values indicate a wider pore size distribution. The n_{DA} value typically ranges between 2 and 10. This range can vary depending on the surface heterogeneity and pore structure of the adsorbent.

A high E value suggests chemisorption, while a low E value is indicative of physisorption [37].

3.2.2.2. Redlich-Peterson (R-P) adsorption isotherm:

The R-P adsorption isotherm is a hybrid model that combines features of the Langmuir and Freundlich isotherms. It is designed to describe adsorption on both homogeneous and heterogeneous surfaces and is particularly effective for systems operating over a wide concentration range.

The isotherm is mathematically expressed as:

$$q_e = \frac{K_{RP} C_e}{1 + \alpha_{RP} C_e^{\beta_{RP}}} \quad (16)$$

where K_{RP} and α_{RP} are the R-P constant (L/g) and R-P energy constant (L/mg or L/mmol), respectively. β_{RP} is the empirical parameter ($0<\beta_{RP}\leq 1$), reflecting the heterogeneity of the adsorbent surface. When $\beta_{RP}=1$, the isotherm reduces to the Langmuir model. When $\beta_{RP}<1$, the isotherm resembles the Freundlich model. Lower β_{RP} values indicate greater surface heterogeneity.

The isotherm can describe adsorption on both homogeneous and heterogeneous surfaces and fits experimental data over a wide concentration range. The R-P isotherm is widely used in liquid-phase adsorption systems, particularly for modeling the adsorption of heavy metal ions, organic pollutants, and other contaminants from aqueous solutions [4,38,39].

3.2.2.3. Sips adsorption isotherm:

The Langmuir and Freundlich isotherms are undoubtedly the most recognized models in adsorption studies. The Sips isotherm integrates features of both models. It was introduced to overcome the limitations of the Freundlich model at higher adsorbate concentrations and to describe adsorption behavior in heterogeneous systems. At low concentrations, the Sips isotherm behaves similarly to the Freundlich model, while at high concentrations, it approaches the Langmuir isotherm.

The mathematical equation of the Sips adsorption isotherm is given in Eq. (17).

$$q_e = \frac{q_m K_S C_e^{\beta_S}}{1 + K_S C_e^{\beta_S}} \quad (17)$$

where K_S is Sips equilibrium constant (L/mg), and β_S is Sips model exponent [32,39].

3.2.2.4. Tóth adsorption isotherm:

In 1971, József Tóth proposed an isotherm model to provide both experimental and mathematical insights into gas adsorption. The Tóth model gained widespread recognition due to its accurate description of adsorption across the entire pressure range, effective parameter interpretation, and its ability to serve as a basis for deriving other isotherm equations [34,40].

The three-parameter Tóth isotherm, an empirical extension of the Langmuir model, was developed to improve alignment with experimental data. It effectively describes adsorption on heterogeneous surfaces at both low and high concentration extremes [4].

While originally formulated for gas adsorption, the Tóth isotherm has also proven applicable to adsorption phenomena in solution [41]. The mathematical expression for the Tóth isotherm is provided in Eq. (18).

$$q_e = \frac{q_m K_T C_e}{[1 + (K_T C_e)^{n_T}]^{\frac{1}{n_T}}} \quad (18)$$

where K_T is the Tóth equilibrium isotherm constant (L/mg), and n_T is a dimensionless parameter. The model simplifies to the Langmuir isotherm when $n_T=1$. Thus, n_T serves as an indicator of the system's heterogeneity; as n_T deviates from 1, the degree of heterogeneity in the adsorption system increases.

3.2.2.5. Brouers–Sotolongo (B-S) isotherm model:

This isotherm is constructed as a modified exponential function to describe adsorption on heterogeneous surfaces, inspired by Langmuir's suggestion to adapt his isotherm for nonuniform adsorbent surfaces. The model assumes that the adsorbent's surface is divided into distinct patches, each containing active sites with identical energy levels. The B-S equation is specifically designed to account for these features, making it suitable for complex adsorption scenarios involving surface heterogeneity.

The mathematical equation of the B-S isotherm model is:

$$q_e = q_m \left[1 - e^{\left(-K_{BS} C_e^{\alpha_{BS}}\right)}\right] \quad (19)$$

where the parameter K_{BS} ensures that the exponential term is dimensionless. Therefore, the unit of K_{BS} must cancel out the unit of $C_e^{\alpha_{BS}}$. If q_e and q_m are expressed in

mg/g, and C_e is in mg/L, then the unit of K_{BS} can be determined as $\left(\frac{L}{mg}\right)^{\alpha_{BS}}$.

The parameter α_{BS} represents the distribution of adsorption energy and reflects the degree of heterogeneity of the adsorbent surface at a specific temperature. It characterizes how adsorption energy varies across different active sites, providing insights into the energy profile and structural diversity of the adsorbent [42,43].

3.3. Error function

Error analysis plays a crucial role in comparing experimental data with theoretical results, as it helps assess the accuracy and reliability of the model. In experimental fields such as adsorption studies, error analyses are used not only to evaluate how well the data fit the model but also to test the accuracy and validity of the model. The choice of error analysis method depends on the nature of the data and the complexity of the model. Generally, a combination of different error analysis methods is preferred to ensure reliable results and to prevent misinterpretations of model performance.

The following section outlines several common error analysis methods, providing concise definitions and their associated formulas [4,16,34,44–49]. The symbols used in these formulas and their meanings are as follows:

- $q_{e,exp,i}$: Experimental adsorption capacity at equilibrium for the *i*-th data point (mg/g).
- $q_{e,cal,i}$: Calculated adsorption capacity at equilibrium for the *i*-th data point based on the model (mg/g)
- $\overline{q}_{e,exp}$: Mean of experimental data (mg/g)
- $\overline{q}_{e,cal}$: Mean of calculated data (mg/g)
- N : Total number of experimental data points.
- p : Number of independent variables in the model.
- R^2 : Coefficient of determination, representing the proportion of variance explained by the model.

3.3.1. Sum of squared errors (SSE)

The sum of squared errors (SSE) provides the total of the squared differences between calculated and experimental data. SSE is used to determine how close the model is to the experimental data. This method minimizes the sum of squared errors to optimize the model parameters.

$$SSE = \sum_{i=1}^{N} \left(q_{e,exp,i} - q_{e,cal,i}\right)^2 \quad (20)$$

SSE is simple to compute and interpret, and SSE offers a clear sense of the total error in the model. However, large errors are disproportionately penalized due to the squaring of the differences by SSE. In addition, SSE should be used in conjunction with other methods for a more comprehensive assessment.

3.3.2. Average relative error (ARE)

ARE is a measure of how well a model predicts experimental data, expressed in terms of the relative error between calculated and experimental values. It evaluates the percentage deviation of calculated values from experimental ones, averaged across all data points.

$$ARE = \frac{1}{N}\sum_{i=1}^{N} \left|\frac{q_{e,exp,i} - q_{e,cal,i}}{q_{e,exp,i}}\right| \times 100 \quad (21)$$

ARE represents the error in percentage form, making it suitable for comparing datasets with different units or scales. It is easy to interpret, as it provides a clear measure of percentage deviation. Unlike RMSE or SSE, ARE does not excessively penalize large errors due to the absence of squaring. However, when $q_{e,exp,i}$ values are small, ARE can become disproportionately large or even undefined. Additionally, larger deviations in $q_{e,exp,i}$ are weighted more heavily due to their relative nature. ARE is also sensitive to outliers and noise in experimental data.

3.3.3. Hybrid fractional error (HYBRID)

The HYBRID function is an error function used to evaluate the accuracy of a model by combining both absolute and fractional errors. It is commonly used in adsorption tests to assess the differences between experimental and calculated values.

$$HYBRID = \frac{1}{N-p}\sum_{i=1}^{N} \left[\frac{\left(q_{e,exp,i} - q_{e,cal,i}\right)^2}{q_{e,exp,i}}\right] \times 100 \quad (22)$$

The HYBRID function combines both absolute and fractional errors, providing a more accurate measure of model performance. It is suitable for datasets with varying magnitudes and scales, and helps penalize errors relative to the experimental values, offering a more balanced evaluation. However, it is sensitive to small or zero values in the experimental data, which can result in inflated error values. Additionally, it can be more complex to interpret compared to simpler metrics like MAE or RMSE.

3.3.4. Marquardt's percent standard deviation (MPSD)

Marquardt's Percent Standard Deviation (MPSD) is an error analysis metric used to evaluate the fit of a model to experimental data. It is particularly useful in adsorption studies, where it helps quantify the deviation between experimental and calculated values in terms of a percentage. MPSD is similar to RMSE but is normalized by the experimental values, making it less sensitive to large magnitudes in the data.

$$MPSD = 100 \times \sqrt{\frac{1}{N-p}\sum_{i=1}^{N}\left(\frac{q_{\mathrm{e,exp},i} - q_{\mathrm{e,cal},i}}{q_{\mathrm{e,exp},i}}\right)^2} \quad (23)$$

MPSD expresses error as a percentage, making it easily interpretable and comparable across different datasets. By accounting for variations in the magnitude of experimental values, it reduces bias from large datasets. MPSD is particularly effective for comparing different models or adsorption isotherms to identify the best fit. However, similar to ARE, MPSD can be disproportionately influenced when $q_{e,exp,i}$ values are small, potentially leading to large errors or undefined values. Additionally, MPSD requires knowledge of the number of parameters (p), making it less straightforward than simpler metrics such as SSE or RMSE. MPSD can also be sensitive to outliers in experimental data.

3.3.5. Mean absolute error (MAE)

MAE calculates the average of the absolute errors between experimental and calculated values. It directly quantifies the magnitude of errors without considering their direction.

$$MAE = \frac{1}{N}\sum_{i=1}^{N}\left|q_{\mathrm{e,exp},i} - q_{\mathrm{e,cal},i}\right| \quad (24)$$

MAE directly represents the magnitude of errors and does not excessively penalize larger errors, offering a balanced approach. However, it does not differentiate between large and small errors in terms of their impact. Additionally, MAE lacks sensitivity to variations in error size across different parts of the data.

3.3.6. Coefficient of determination (R^2)

R^2 measures how well the model explains the variance in the data. A value close to 1 indicates a good fit, while values near 0 suggest poor model performance. The coefficient of determination (R^2) is also equal to the square of the correlation coefficient (R).

$$R^2 = \left[\frac{\sum\left(q_{\mathrm{e,exp},i} - \overline{q}_{\mathrm{e,exp}}\right)\left(q_{e,cal,i} - \overline{q}_{\mathrm{e,cal}}\right)}{\sqrt{\sum\left(q_{\mathrm{e,exp},i} - \overline{q}_{\mathrm{e,exp}}\right)^2 \sum\left(q_{\mathrm{e,cal},i} - \overline{q}_{\mathrm{e,cal}}\right)^2}}\right]^2 \quad (25)$$

R^2 provides a quick measure of model accuracy and is both widely used and easily interpretable. However, it can be misleading for non-linear data or when the model is poorly specified. A high R^2 value does not necessarily guarantee accurate predictions, particularly for non-linear models.

3.3.7. Adjusted R-squared (Adjusted R^2 or R^2-adj)

The Adjusted R^2 statistic is used to evaluate the goodness of fit of a model (e.g., isotherm or kinetic model) to the experimental q_e data. It adjusts for the number of parameters in the model, providing a more accurate assessment of how well the model describes the adsorption process while penalizing unnecessary complexity.

$$R^2\text{-adj} = 1 - \left[\frac{(1-R^2)(N-1)}{N-p-1}\right] \quad (26)$$

Adjusted R^2 prevents overfitting by accounting for the number of parameters, allows for better comparison between different adsorption models, and provides a more reliable measure of model fit. However, Adjusted R^2 is still sensitive to outliers, does not imply causality, and can be difficult to interpret in complex models.

4. Results and discussions

4.1. Minimization process with Excel Solver

Fig. 1 and Fig. 2 illustrate the minimization process for non-linear regression solutions in Excel Solver. Fig. 1 demonstrates the minimization/optimization process in the Solver using the HYBRID function for the two-parameter Langmuir isotherm. Fig. 2 illustrates the process for the three-parameter Redlich-Peterson (R-P) model using the SSE function.

In the Excel sheet, follow the sequence: **File – More options – Options – Add-ins – Solver Add-in** to add the Solver command to the menus. Then, navigate to the **Data** tab and run the Solver command.

In columns A and B in Fig. 1 and Fig. 2, the experimental C_e ($C_{e,exp}$) and corresponding experimental q_e values ($q_{e,exp}$) are placed. Column C represents the q_e values ($q_{e,cal}$) calculated by the model at the end of the process. Columns D and E contain the calculations for the error function, which minimizes the differences between $q_{e,exp}$ and $q_{e,cal}$.

In Fig. 1, Cells A14 and B14 contain the Langmuir model constants (K_L and q_m). The primary objective of the minimization process is to estimate these constants with the highest accuracy. To achieve this, the error function seeks to minimize the differences between $q_{e,exp}$ and $q_{e,cal}$. In other words, K_L and q_m values must be assigned to cells A14 and B14 such that the error function value in cell E14 is minimized.

Before running Solver, it is necessary to assign initial estimates to cells A14 and B14. (A14, B14, and C14 in Fig. 2) This is because Solver cannot operate if these cells are empty, as the calculated $q_{e,cal}$ values (C3–C11) would be undefined. Once initial estimates are assigned, Solver will use a trial-and-error method to minimize the differences between $q_{e,exp}$ and $q_{e,cal}$ through the selected error function, ultimately determining the most accurate values for K_L and q_m (K_{RP}, α_{RP}, and β_{RP} for R-P isotherm in Fig. 2).

Once the necessary cells are filled, Solver is run, and the "**Solver Parameters**" dialog box appears on the screen, as shown in Fig. 1 and Fig. 2. Click the arrow button next to the "**Set Objective**" bar and select the cell containing the value of the error function to be minimized (E14) as the target. Since error functions perform minimization, select the "**Min**" option in the dialog box.

Next, click the arrow button to the right of the "**By Changing Variable Cells**" bar and select the model parameters cells (A14:B14 for the Langmuir model, A14:C14 for the R-P model). If there are any constraints related to the model, as in the R-P model shown in Fig. 2, click "**Add**" under the "**Subject to the Constraints**" section and enter the necessary constraints in the window that appears. The constraints will be displayed in the dialog box (Fig. 2).

Since a non-linear solution is being performed, select "**GRG Nonlinear**" from the list under "**Select a Solving Method**" in the dialog box. Finally, click the "**Solve**" button to allow Solver to perform the minimization and estimate the $q_{e,cal}$ values and the model parameters.

Similar steps are, of course, applied to kinetic data as well. In this case, experimental t (min) values are entered into cells A3–A11, and experimental $q_{t,exp}$ values are entered into cells B3–B11. The remaining steps are carried out as described above.

4.2. Error function analysis for the kinetics models

Error functions are tools that help accurately estimate model parameters. These functions work to minimize the difference between experimental data and data calculated from the model as much as possible.

In this study, five different error functions were employed for data minimization: SSE, ARE, HYBRID, MPSD, and MAE. Table 1 presents the results of minimization performed using these five error functions with Solver for each kinetic model. The rows detail the parameter values obtained for each kinetic model using the respective error function. For example, when minimization for the PFO kinetic model was conducted with SSE in Solver, the q_t value was 10.15784 mg/g, while it was 10.41159 mg/g with ARE, 9.89718 mg/g with HYBRID, 9.35466 mg/g with MPSD, and 10.41206 mg/g with MAE.

In the respective tables, error function values are also provided both vertically and horizontally. When the same error function is aligned vertically and horizontally in these tables, the value read in the intersecting cell represents the result obtained when the solution is performed under that error function. For instance, in Table 1, when the horizontal SSE is aligned with the vertical SSE, the intersecting cell value is 5.61275. However, when the horizontal SSE aligns with the vertical ARE, the intersecting cell value becomes 9.41517. This value (9.41517) represents the ARE calculated under SSE minimization conditions, where the $q_{e,cal}$ values estimated via SSE are substituted into the mathematical equation for ARE. This approach was used to generate the values in Table 1, Table 3, and Table 4. As shown, each function provides the lowest minimization under its specific conditions.

At the end of Table 1, Table 3, and Table 4, SNE (Sum of Normalized Errors) values are provided for each model. SNE is a normalization process that identifies which error function minimizes the differences between qe,exp and qe,cal the most. Thus, SNE helps determine the most appropriate error function for a given model and allows for a more accurate prediction of the compatibility of experimental data with the model.

An example of SNE calculation from Table 1 is as follows: The error function values in each row are divided by the largest value in that row, resulting in five different normalized values (note that one of these values will always equal 1). The same process is repeated for the other four rows. Finally, the SNE value for each error function is obtained by summing up the normalized values for each column.

The error function with the relatively smallest SNE value is the one that should be preferred for the minimization of the corresponding model in Solver.

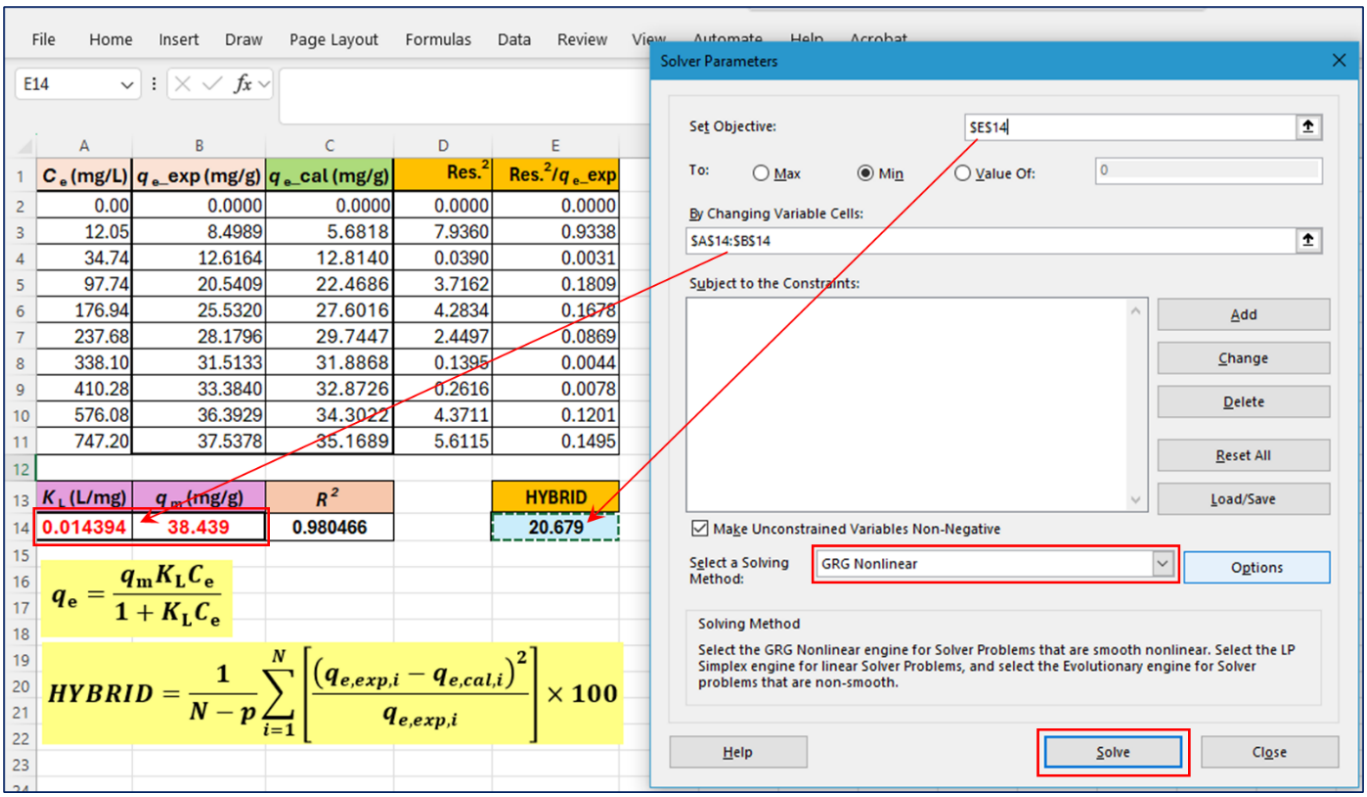

C_e (mg/L)	q_e_exp (mg/g)	q_e_cal (mg/g)	Res.^{2}	Res.^{2}/q_e_exp
0.00	0.0000	0.0000	0.0000	0.0000
12.05	8.4989	5.6818	7.9360	0.9338
34.74	12.6164	12.8140	0.0390	0.0031
97.74	20.5409	22.4686	3.7162	0.1809
176.94	25.5320	27.6016	4.2834	0.1678
237.68	28.1796	29.7447	2.4497	0.0869
338.10	31.5133	31.8868	0.1395	0.0044
410.28	33.3840	32.8726	0.2616	0.0078
576.08	36.3929	34.3022	4.3711	0.1201
747.20	37.5378	35.1689	5.6115	0.1495

K_L (L/mg)	q_m (mg/g)	R^2	HYBRID
0.014394	38.439	0.980466	20.679

Figure 1. Optimization and solution of the two-parameter Langmuir isotherm model using the HYBRID error function in Excel Solver

- The q_e_cal values in cells C3–C11 are calculated in Excel using the Langmuir equation as follows: =($B$14*$A$14*A3)/(1+$A$14*A3), =($B$14*$A$14*A4)/(1+$A$14*A4), …. =($B$14*$A$14*A11)/(1+$A$14*A11)
- In cells D3–D11, the squares of the differences (Res.^{2}) between q_e_exp and q_e_cal are calculated (e.g., =(B3-C3)^2, =(B4-C4)^2, ..., =(B11-C11)^2). In cells E3–E11, the values in D3–D11 are divided by the q_e_exp values in B3–B11 (e.g., =D3/B3, =D4/B4, ..., =D11/B11); HYBRID=SUM(E3:E11).
- Coefficient of determination, R^2 =RSQ(B2:B11;C2:C11)

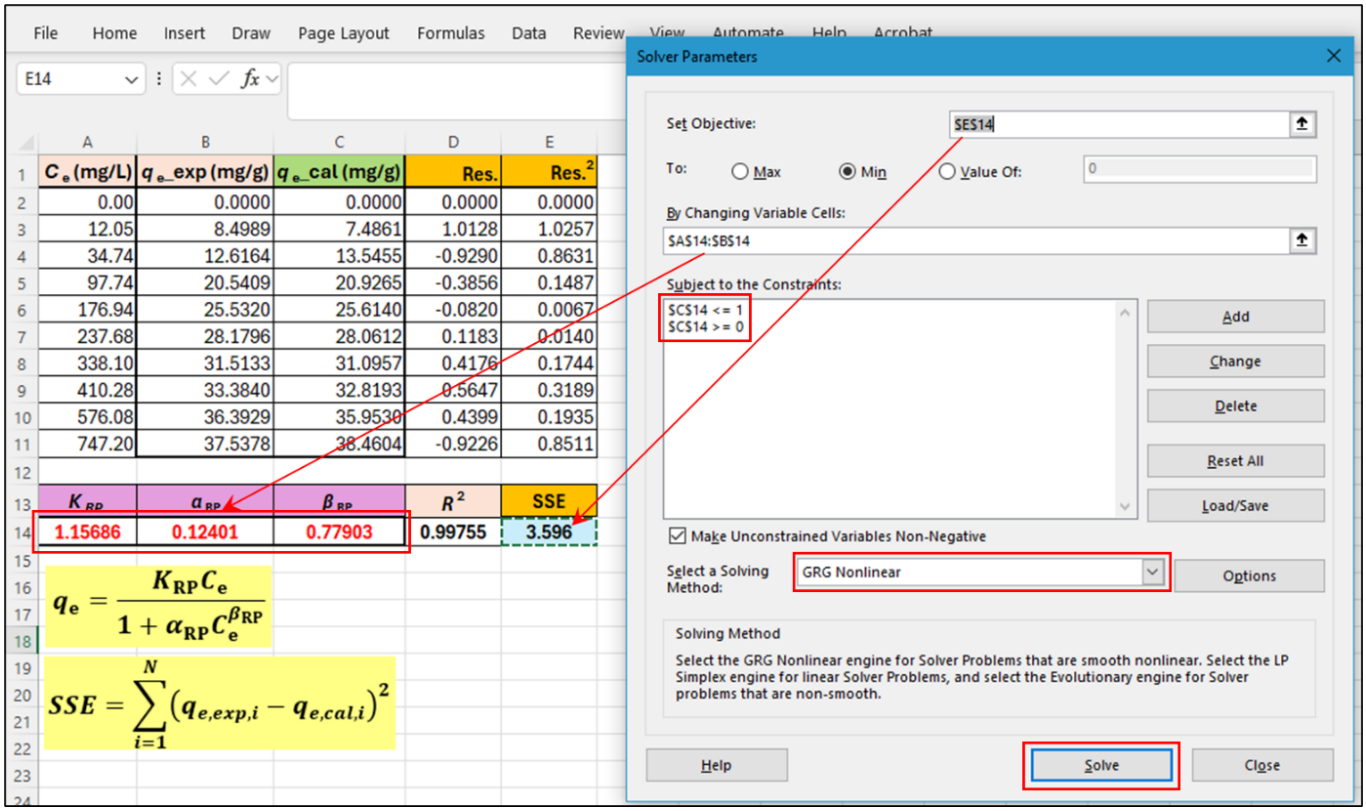

C_e (mg/L)	q_e_exp (mg/g)	q_e_cal (mg/g)	Res.	Res.^{2}
0.00	0.0000	0.0000	0.0000	0.0000
12.05	8.4989	7.4861	1.0128	1.0257
34.74	12.6164	13.5455	-0.9290	0.8631
97.74	20.5409	20.9265	-0.3856	0.1487
176.94	25.5320	25.6140	-0.0820	0.0067
237.68	28.1796	28.0612	0.1183	0.0140
338.10	31.5133	31.0957	0.4176	0.1744
410.28	33.3840	32.8193	0.5647	0.3189
576.08	36.3929	35.9530	0.4399	0.1935
747.20	37.5378	38.4604	-0.9226	0.8511

K_{RP}	α_{RP}	β_{RP}	R^2	SSE
1.15686	0.12401	0.77903	0.99755	3.596

Figure 2. Optimization and solution of the three-parameter Redlich-Peterson (R-P) isotherm model using the SSE error function in Excel Solver

- The q_e_cal values in cells C3–C11 are calculated in Excel using the Redlich-Peterson equation as follows: =($A$14*A3)/(1+$B$14*(A3^$C$14)), =($A$14*A4)/(1+$B$14*(A4^$C$14)), …. , =($A$14*A11)/(1+$B$14*(A11^$C$14))
- Res. (Residuals) are calculated as the differences between q_e_exp and q_e_cal (e.g., =B3-C3, =B4-C4, ..., =B11-C11). Then, the squares of these differences are calculated in cells E3–E11 (e.g., =D3^2, D4^2, …. D11^2). SSE is ultimately the sum of the squares of these differences; SSE=SUM(E3:E11).
- Determination coefficient, R^2 =RSQ(B2:B11;C2:C11)

Table 1. Kinetic model constants with five different error analysis in Microsoft Excel Solver

Kinetic models	SSE	ARE	HYBRID	MPSD	MAE
Pseudo-first order (PFO)					
q_t (mg/g)	10.15784	10.41159	9.89718	9.35466	10.41206
k_1 (1/min)	0.07023	0.09935	0.09186	0.13775	0.06720
R^2	0.96996	0.95218	0.95737	0.92437	0.97119
R^2–Adj	0.96138	0.93851	0.94519	0.90276	0.96295
SSE	**5.61275**	9.41517	6.62396	11.79655	5.98032
ARE	13.35946	**12.29921**	13.02401	14.70117	13.18084
HYBRID	17.16781	19.09022	**15.13926**	19.54712	18.12834
MPSD	25.19315	21.47662	21.60214	**19.18431**	25.66247
MAE	0.63672	0.70318	0.73162	1.00242	**0.59712**
SNE	3.87970	4.14975	**3.79357**	4.74756	3.92664
Pseudo-second order (PSO)					
q_t (mg/g)	10.78276	10.89592	10.57112	10.16293	10.91555
k_2 (g/mg·min)	0.01020	0.01097	0.01250	0.01689	0.01052
R^2	0.99369	0.99236	0.98997	0.97969	0.99307
R^2–Adj	0.99188	0.99018	0.98710	0.97389	0.99109
SSE	**1.15192**	1.49209	1.49687	3.29579	1.38196
ARE	6.75051	**6.23831**	6.76816	8.41013	6.39992
HYBRID	5.14998	4.89708	**4.34811**	5.97884	5.01204
MPSD	15.58695	14.10526	12.88466	**11.20023**	14.69183
MAE	0.27226	0.27191	0.34589	0.54170	**0.26400**
SNE	3.51614	**3.42046**	3.45134	4.71856	3.44851
Elovich					
α_E (mg/g·min)	5.81997	3.30410	4.19424	3.57695	7.57775
β_E (g/mg)	0.64626	0.55775	0.60294	0.57811	0.65356
R^2	0.98244	0.97774	0.98081	0.97905	0.98223
R^2–Adj	0.97743	0.97138	0.97533	0.97306	0.97715
SSE	**2.59144**	4.14707	2.92915	3.43097	3.62022
ARE	8.07160	**5.31391**	6.43614	5.67360	9.49963
HYBRID	5.49977	5.34174	**4.30429**	4.62875	9.80496
MPSD	12.44534	7.54710	7.98919	**7.27624**	18.55071
MAE	0.46489	0.48227	0.47149	0.47828	**0.45524**
SNE	3.67031	3.51102	**3.23113**	3.28062	4.81691
Avrami					
k_A ($\mathbf{min^{-n_A}}$)	0.20583	0.19139	0.19721	0.19300	0.19618
n_A	0.54050	0.56350	0.55483	0.56390	0.55076
R^2	0.99906	0.99887	0.99899	0.99891	0.99889
R^2–Adj	0.99880	0.99854	0.99870	0.99860	0.99858
SSE	**0.14050**	0.18638	0.15811	0.18733	0.16781
ARE	1.70353	**1.04928**	1.27732	1.19222	1.16089
HYBRID	0.33165	0.29921	**0.27052**	0.28954	0.30130
MPSD	3.04051	1.99572	2.09374	**1.93974**	2.18486
MAE	0.08498	0.08555	0.08379	0.09397	**0.07696**
SNE	4.65432	4.07985	**3.98981**	4.21085	4.02343
Brouers-Sotolongo (B-S)					
q_t (mg/g)	11.07665	11.06952	11.09914	11.14210	11.07287
τ_c (min)	13.22303	13.21365	13.17745	13.04019	13.22493
α_{BS}	0.64608	0.63511	0.64283	0.63573	0.64583
n_{BS}	1.47640	1.48059	1.47811	1.46878	1.47454
$\tau_{1/2}$ (min)	9.74988	9.71516	9.71075	9.52562	9.73986
R^2	0.99958	0.99955	0.99957	0.99954	0.99956
R^2–Adj	0.99915	0.99910	0.99914	0.99907	0.99912
SSE	**0.06234**	0.07943	0.06296	0.06825	0.07532
ARE	1.11769	**0.90266**	1.06123	0.96652	1.09833
HYBRID	0.12815	0.15190	**0.12697**	0.13233	0.15316
MPSD	1.63236	1.63037	1.57112	**1.52857**	1.84393
MAE	0.06708	0.06209	0.06576	0.06344	**0.06150**
SNE	4.50677	4.60932	4.40352	**4.36279**	4.84779

Accordingly, based on the SNE data in Table 1 and Table 2, the HYBRID error function provides the best minimization for all kinetic models except for PSO and B-S. For PSO and B-S, the most suitable minimizations are achieved using ARE and MPSD, respectively. Based on the SNE values of the kinetic models presented in Table 1, the ranking of error functions from best to worst can be determined as follows: for PFO, HYBRID > SSE > MAE > ARE > MPSD; for PSO, ARE > MAE > HYBRID > SSE > MPSD; for Elovich, HYBRID > MPSD > ARE > SSE > MAE; for Avrami, HYBRID > MAE > ARE > MPSD > SSE; and for B-S, MPSD > SSE > HYBRID > ARE > MAE.

Fig. 3 illustrates the $t-q_t$ plots obtained for each model when analyzed separately in Solver using five different error functions. As illustrated in Fig. 3, for PFO and PSO kinetic models, MPSD is not regarded as a suitable minimization function in Excel Solver when compared to other error functions. Table 1 also demonstrates that the SNE values for MPSD in PFO and PSO kinetic models are significantly higher relative to the other error functions. Notably, the Avrami and B-S kinetic models exhibit consistent trends across all error functions. In particular, for the B-S kinetic model, the $q_{t,cal}$ values obtained from each error function are remarkably close to each other, with their respective curves nearly overlapping entirely.

Consequently, it is evident that selecting an appropriate error function is crucial for non-linear solutions of the PFO kinetic model, as well as for the PSO and Elovich kinetic models. However, this choice is less critical for the Avrami and B-S kinetic models.

Another noteworthy point in Table 1 is that all error function values for the B-S model are the lowest among all models. Relatively low error function values indicate that the $q_{t,exp}$ and $q_{t,cal}$ values are very close to each other, signifying that the corresponding model represents the experimental data exceptionally well.

As seen in Fig. 3, the experimental data is best represented by the B-S model, followed by the Avrami model. Fig. 4 further supports this conclusion, providing a visual representation of the $t-q_t$ plots drawn using the error functions with the lowest relative SNE values (Table 2). As illustrated in Fig. 4, the kinetic models that best represent the experimental data are, in order, the B-S and Avrami kinetic models. The PSO kinetic model, on the other hand, ranks as the third most suitable model in this analysis. However, it can also be stated that both the Elovich and PFO kinetic models fail to adequately represent the experimental data.

Fig. 5 presents the detailed version of Fig. 4, showing the results for each model individually. As is evident from the figure, the two models that best represent the data are the B-S and Avrami models. Likewise, Fig. 5 suggests that the PSO kinetic model can be considered a suitable model for adequately representing the experimental data.

In conclusion, based on the relevant tables and graphs, the kinetic model that best describes the adsorption of Pb^{2+} onto pine bark is the Brouers-Sotolongo (B-S) model, while the least representative model is the pseudo-first order (PFO) kinetic model.

4.3. Analysis of the kinetics model constants

In **Section 3.1.5**, it was stated that the 4-parameter B-S kinetic model provides a more precise and accurate description of the adsorption kinetics process compared to the classical PFO and PSO models, owing to its consideration of additional factors such as a fractal time parameter (α_{BS}) and a fractional order parameter (n_{BS}).

In this study, based on the data presented in Table 1, the α_{BS} value for the B-S kinetic model is 0.63573 (obtained through MPSD minimization). This value ($\alpha_{BS} < 1$) indicates that the system is significantly heterogeneous, reflecting the heterogeneity of the pine bark surface. Additionally, the n_{BS} value derived from Table 1 is 1.46878. When $n_{BS} = 1$, the system follows PFO kinetics, whereas $n_{BS} = 2$ indicates PSO kinetics. Given that $1 < n_{BS} < 2$ for this study, it can be concluded that a mixed kinetic mechanism is at play, where adsorption occurs as a combination of physical and chemical interactions. On the other hand, for $0 < n_{BS} < 1$, adsorption proceeds predominantly through physical mechanisms. Consequently, the reaction order and pathway can be determined with greater precision using the B-S kinetic model.

$\tau_{1/2}$ represents the time required for half of the total adsorbed adsorbate ions/molecules to be adsorbed during the adsorption process. For this study, this duration is $\tau_{1/2} = 9.74988$ minutes (Table 1).

For the Avrami kinetic model, which was determined to be consistent with the experimental data, an examination of the model constants in Table 1 reveals that the n_A exponent, which provides information about the adsorption mechanism and geometry, is 0.55483 (obtained through minimization using the HYBRID error function). When $0 < n_A < 1$, it indicates that adsorption progresses through physical pathways on heterogeneous surfaces with limited and weak interactions.

Another parameter of the Avrami model, k_A, being less than 1 (in this study, $k_A \approx 0.2$) suggests that the adsorption process has relatively slow kinetics, with a low adsorption rate, or that one or more steps in the process are rate-limiting.

Unlike PFO, what perhaps makes the PSO kinetic model more appealing in many studies is the overlap between $q_{t,exp}$ and the $q_{t,cal}$ values. It should be noted,

however, that the choice of the error function type is crucial when performing analyses with PFO and PSO. When Fig. 3 is carefully examined, it becomes evident that the selection of the error function for PFO is critical. In Fig. 3, when MPSD is chosen as the error function for both PFO and PSO, neither model yields particularly reliable results. Therefore, identifying the error function that provides the most accurate results is essential. This study focuses specifically on this objective. However, when ARE or MAE is preferred for both models, the difference between $q_{t,exp}$ and the $q_{t,cal}$ values becomes significantly smaller (Table 1, Fig. 3). Nevertheless, in Table 1 and Table 2, the most optimal error function for PFO is found to be HYBRID. This is due to the sharper inflection point of the t–q_t curve in ARE and MAE, as well as the experimental data in this region being farther from the curve (Fig. 3). It can be observed from Fig. 3 that the Elovich kinetic model does not align well with the data, particularly near equilibrium. Although the Elovich model does not represent the experimental data in a fully satisfactory manner, certain interpretations can still be derived from the model constant values. Based on the values obtained using HYBRID minimization in Table 1, the α_E value for the Elovich model is 4.19424, and the β_E value is 0.60294. When $\alpha_E > 1$, it indicates that adsorption is quite rapid at the initial stages, suggesting strong interactions between the adsorbent and the adsorbate. Additionally, when $\beta_E > 0.5$, a more pronounced slowing of the adsorption rate is observed, indicating that active sites are filling up quickly.

4.4. Error function analysis for the isotherm models

A similar evaluation to the one conducted for kinetic models can undoubtedly be performed for isotherm models as well. Table 3 lists the minimization results obtained using five different error functions in Excel Solver for two-parameter isotherms, while Table 4 provides the corresponding results for three-parameter isotherms.

When evaluating the SNE values collectively presented in Table 5, it can be observed that many two- and three-parameter isotherm models are better minimized using the HYBRID error function. For the Temkin model, SSE; for the D-R model, ARE and SSE; and for the Jovanovic and D-A models, ARE provided better minimization results. In contrast, for the remaining models, the HYBRID function yielded the best minimization results. Overall, for both kinetic and isotherm models, the HYBRID error function generally offered superior minimization performance.

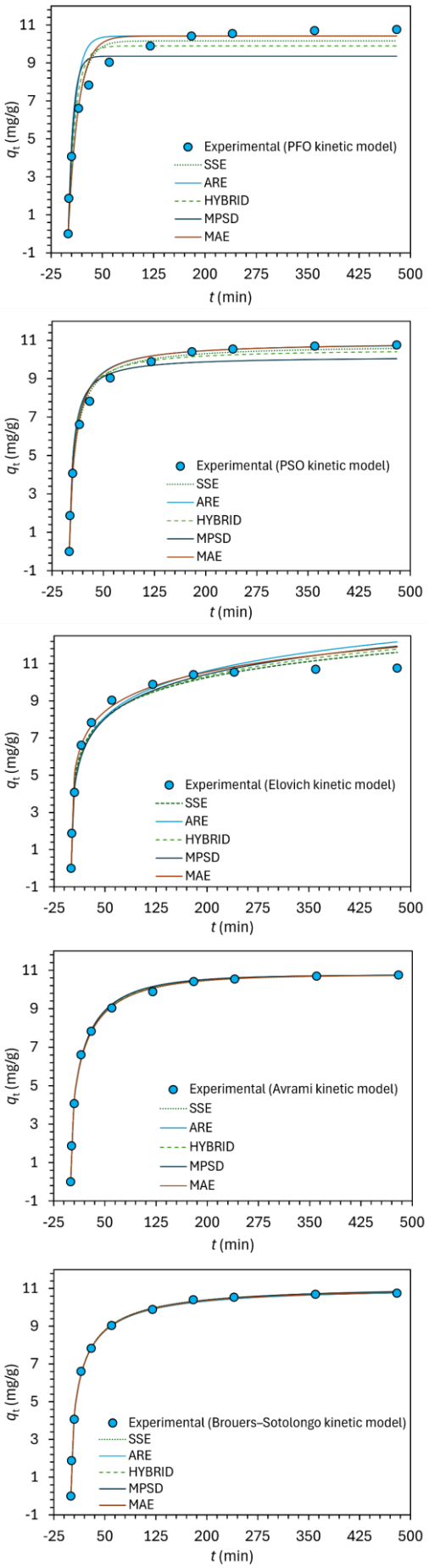

Figure 1. Comparison of experimental and model-predicted kinetic data using five different error functions (SSE, ARE, HYBRID, MPSD, and MAE) in Excel Solver for various kinetic models

Table 2. SNE values of the error functions for the kinetic models

	SNE values of the error functions				
Kinetic models	**SSE**	**ARE**	**HYBRID**	**MPSD**	**MAE**
Pseudo-first order (PFO)	3.87970	4.14975	**3.79357**	4.74756	3.92664
Pseudo-second order (PSO)	3.51614	**3.42046**	3.45134	4.71856	3.44851
Elovich	3.67031	3.51102	**3.23113**	3.28062	4.81691
Avrami	4.65432	4.07985	**3.98981**	4.21085	4.02343
Brouers-Sotolongo (B-S)	4.50677	4.60932	4.40352	**4.36279**	4.84779

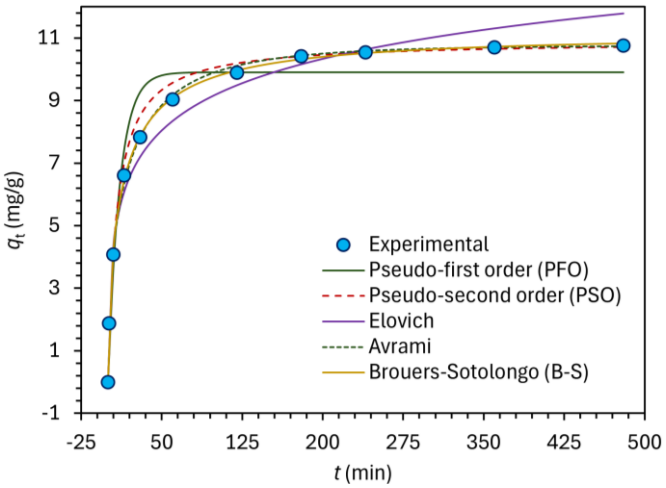

Figure 2. Comparison of the kinetic models optimized in Excel Solver

Fig. 6 and Fig. 7 illustrate the C_e–q_e plots for each isotherm model, generated by minimizing the differences between $q_{e,exp}$ and $q_{e,cal}$ using five error functions in Solver. In Fig. 6, except for the D-R and Jovanovic models, the C_e–q_e graphs generated for the other two-parameter isotherms after minimization with the five error functions are quite similar to each other. However, as with the kinetic models, the MPSD function provided poorer minimization results compared to the others. Similarly, in Fig. 7, for the four isotherms other than the D-A isotherm, the results obtained from the five error functions were closely aligned.

From the SNE data in Table 3, Table 4, and Table 5, the error functions providing the best minimization results are as follows: for the Temkin model, SSE; for the D-R, Jovanovic, and D-A models, ARE; and for all other isotherms, the HYBRID function. Additionally, the same tables reveal that MPSD yielded the highest SNE values for the Freundlich and Temkin isotherms.

Unlike the two-parameter isotherms, the three-parameter isotherms produced more consistent results across the five error functions, as illustrated in Fig. 7. For the three-parameter isotherms other than D-A, the five error functions provided nearly identical results, with all C_e–q_e graphs almost entirely overlapping. Therefore, the choice of error function for minimizing these three-parameter isotherms, excluding D-A, is not critical.

To ensure more accurate parameter estimation and, consequently, a better understanding of the adsorption process, it is essential to select the error function with the smallest SNE value for minimizing each isotherm model, as summarized in Table 5.

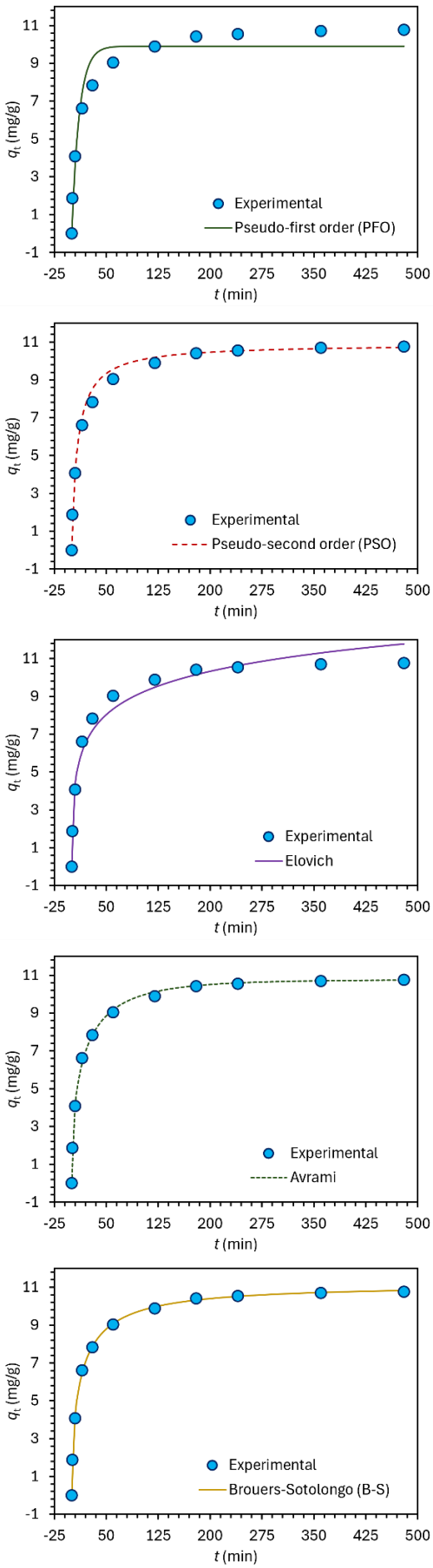

Figure 3. Single representations of the kinetic models optimized in Excel Solver

Table 3. Two-parameter isotherms constants with five different error analysis in Microsoft Excel Solver

	SSE	ARE	HYBRID	MPSD	MAE
Langmuir					
K_L (L/mg)	0.01116	0.01428	0.01439	0.01863	0.01003
q_m, (mg/g)	40.69627	38.04907	38.43876	35.98128	41.49816
R^2	0.98715	0.98075	0.98047	0.96900	0.98859
R^2–Adj	0.98286	0.97433	0.97396	0.95866	0.98478
SSE	**22.87550**	30.00669	28.80803	49.32668	24.09545
ARE	7.57277	**7.00233**	7.25302	8.60763	7.70209
HYBRID	24.73757	21.10073	**20.67920**	25.11808	29.12894
MPSD	16.05378	13.26780	13.04970	**11.87321**	17.72985
MAE	1.15155	1.35836	1.39217	1.88286	**1.04587**
SNE	3.70984	3.61598	**3.61199**	4.53198	3.93875
Freundlich					
K_F (L/mg)	4.33510	3.23827	3.81191	3.48659	4.35667
n_F (mg/g)	2.98694	2.57897	2.80287	2.68231	2.95498
R^2	0.99068	0.98454	0.98910	0.98704	0.99053
R^2–Adj	0.98758	0.97939	0.98547	0.98272	0.98738
SSE	**13.85285**	29.56261	16.12031	20.74284	18.78967
ARE	5.19552	**3.67535**	4.55495	4.11212	4.95398
HYBRID	9.23253	10.93279	**7.42953**	8.27996	11.56317
MPSD	8.29636	5.82268	5.94497	**5.40667**	9.16491
MAE	0.97761	1.10162	1.04825	1.08950	**0.89804**
SNE	4.05970	4.28821	**3.66474**	3.78812	4.40430
Temkin					
K_M (L/mg)	0.19314	0.29209	0.22476	0.25643	0.13608
b_M (mg/g)	331.07572	367.02597	346.77202	364.91014	305.20117
R^2	0.99150	0.98840	0.99105	0.99000	0.98883
R^2–Adj	0.98866	0.98453	0.98807	0.98666	0.98510
SSE	**12.37752**	20.91711	14.16483	21.68239	22.03380
ARE	5.74074	**5.29550**	5.59892	5.72607	6.25771
HYBRID	12.03239	14.54045	**10.56052**	12.12317	30.31467
MPSD	10.62228	9.68113	8.93485	**8.43623**	18.71355
MAE	0.89423	1.11944	1.01901	1.23140	**0.74194**
SNE	**3.16987**	3.70161	3.19093	3.74981	4.60252
Dubinin-Radushkevich (D-R)					
q_m (mg/g)	31.87089	31.83077	30.76107	29.51396	31.83077
K_{DR} (mol²/kJ²)	0.00025	0.00019	0.00020	0.00018	0.00019
R^2	0.87572	0.86254	0.86704	0.85890	0.86254
R^2–Adj	0.83429	0.81672	0.82272	0.81186	0.81672
SSE	**217.06002**	225.37728	225.17758	250.99127	225.37728
ARE	22.04778	**20.17248**	21.05657	20.48773	20.17248
HYBRID	178.33015	178.75627	**173.45011**	177.60889	178.75627
MPSD	39.65376	39.23137	38.80529	**38.59592**	39.23137
MAE	3.83446	3.65788	3.87830	3.97469	**3.65788**
SNE	4.82714	**4.72253**	4.77686	4.89615	4.72253
Jovanovic					
K_J (L/mg)	0.00853	0.00944	0.01170	0.01692	0.00849
q_m (mg/g)	35.14928	34.09320	33.21288	30.80221	34.44130
R^2	0.97164	0.96662	0.95154	0.91493	0.97183
R^2–Adj	0.96219	0.95550	0.93539	0.88657	0.96244
SSE	**59.50168**	62.20115	75.24534	130.46033	62.53696
ARE	12.49796	**11.75927**	12.01660	12.85726	12.47312
HYBRID	59.03252	55.01072	**50.27353**	61.79123	61.59891
MPSD	23.95852	22.67810	19.79322	**17.73674**	24.47825
MAE	1.98414	1.94592	2.32689	2.98063	**1.93578**
SNE	4.02794	**3.86097**	3.91426	4.72459	4.09582

Table 4. Three-parameter isotherms constants with five different error analysis in Microsoft Excel Solver

	SSE	ARE	HYBRID	MPSD	MAE
Dubinin-Astakhov (D-A)					
q_m (mg/g)	36.28594	35.04878	33.01061	29.89269	35.04883
E (J/mol)	1740.32884	2370.09386	4451.71100	8034.88356	2370.07518
n_{DA}	1.00000	1.00000	1.00000	1.00000	1.00000
R^2	0.94460	0.93697	0.91760	0.89393	0.93697
R^2–Adj	0.91136	0.89915	0.86815	0.83030	0.89915
SSE	**97.34395**	100.55178	124.23476	204.90305	100.55154
ARE	15.25030	**13.82581**	15.44667	15.65526	13.82583
HYBRID	112.40611	100.25168	**89.25787**	107.71588	100.25194
MPSD	33.73092	30.76576	25.23452	**22.75592**	30.76584
MAE	2.43443	2.41772	3.04288	3.66897	**2.41772**
SNE	4.11272	**3.83680**	3.96452	4.63291	3.83680
Redlich-Peterson (R-P)					
K_{RP} (L/g)	1.15686	1.83274	1.50019	2.05691	1.06898
α_{RP} (L/mg)	0.12401	0.25510	0.19890	0.34257	0.11967
β_{RP}	0.77903	0.73916	0.74688	0.71147	0.76908
R^2	0.99755	0.99674	0.99711	0.99558	0.99734
R^2–Adj	0.99608	0.99478	0.99538	0.99292	0.99574
SSE	**3.59616**	5.46455	4.21248	6.55358	4.89234
ARE	2.85815	**2.15054**	2.58705	2.63208	2.69613
HYBRID	3.43104	3.83036	**2.90971**	3.45425	4.56374
MPSD	5.50514	4.88051	4.39294	**4.03415**	6.56932
MAE	0.48725	0.45206	0.51910	0.61325	**0.42101**
SNE	3.93307	3.90563	**3.70067**	4.29188	4.37635
Sips					
q_m (mg/g)	59.29319	72.03273	64.01559	71.94951	63.07625
K_S (L/mg)	0.03439	0.03615	0.03531	0.03444	0.03298
β_S	0.59838	0.52561	0.56595	0.53194	0.58558
R^2	0.99897	0.99838	0.99884	0.99831	0.99886
R^2–Adj	0.99836	0.99740	0.99814	0.99730	0.99817
SSE	**1.50396**	2.81605	1.68900	2.46553	2.12054
ARE	1.78491	**1.32273**	1.63663	1.79113	1.61391
HYBRID	1.42883	1.84973	**1.27027**	1.46051	1.60914
MPSD	3.55774	3.32658	3.02625	**2.84654**	3.58978
MAE	0.30239	0.28083	0.31194	0.39150	**0.26307**
SNE	4.06653	4.38250	**3.84006**	4.45807	4.19596
Tóth					
q_m (mg/g)	78.99030	87.54891	99.49835	149.45298	84.73605
K_T (L/mg)	0.31601	0.32634	0.42686	0.57620	0.30829
n_T	0.35793	0.34153	0.29781	0.23384	0.35192
R^2	0.99853	0.99836	0.99831	0.99747	0.99837
R^2–Adj	0.99765	0.99738	0.99730	0.99594	0.99740
SSE	**2.15017**	2.91173	2.46090	3.71978	2.95932
ARE	2.16364	**1.96322**	1.99460	2.10850	2.00727
HYBRID	2.05032	2.47813	**1.79285**	2.09525	2.66427
MPSD	4.25420	4.68729	3.53843	**3.29990**	4.95859
MAE	0.36618	0.30745	0.38921	0.47329	**0.30643**
SNE	3.97924	4.21515	**3.79232**	4.42643	4.37074
Brouers–Sotolongo (B-S)					
q_m (mg/g)	45.03682	51.10940	46.66169	49.60118	49.25654
K_{BS} [(L/mg)$^{\alpha}$]	0.04954	0.05273	0.05101	0.05113	0.05077
α_{BS}	0.54724	0.49742	0.52976	0.50955	0.51526
R^2	0.99930	0.99871	0.99922	0.99887	0.99897
R^2–Adj	0.99888	0.99794	0.99875	0.99819	0.99835
SSE	**1.02876**	2.28147	1.13739	1.64635	1.83074
ARE	1.49086	**1.13223**	1.39978	1.56782	1.24023
HYBRID	1.04753	1.52039	**0.95228**	1.08274	1.18017
MPSD	3.10315	3.03517	2.72203	**2.58492**	2.70323
MAE	0.24226	0.23513	0.24984	0.32666	**0.22761**
SNE	3.83243	4.42005	**3.65970**	4.26676	3.93762

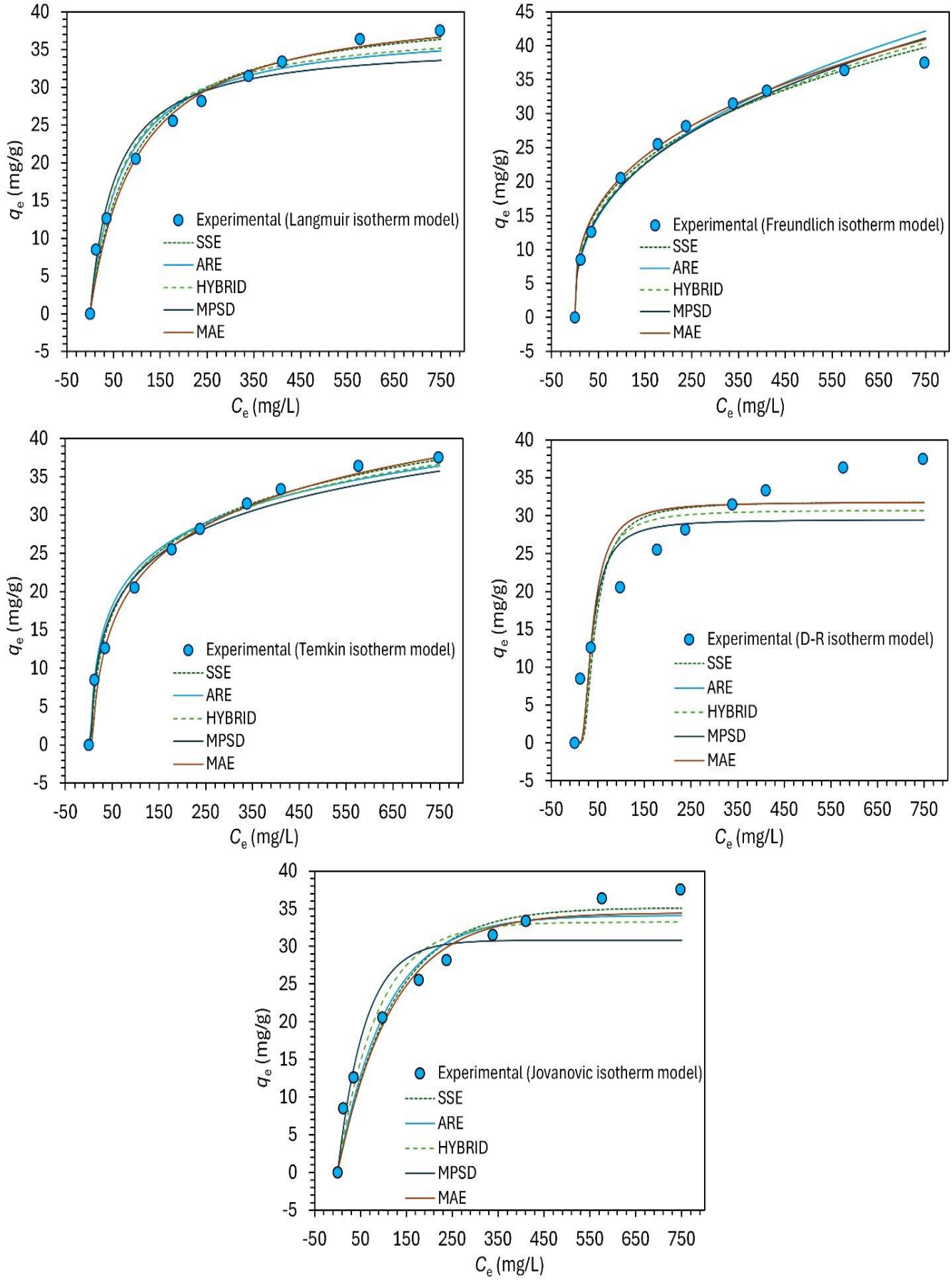

Figure 4. Comparison of experimental and model-predicted adsorption isotherm data using five different error functions (SSE, ARE, HYBRID, MPSD, and MAE) in Excel Solver for two-parameter isotherm models

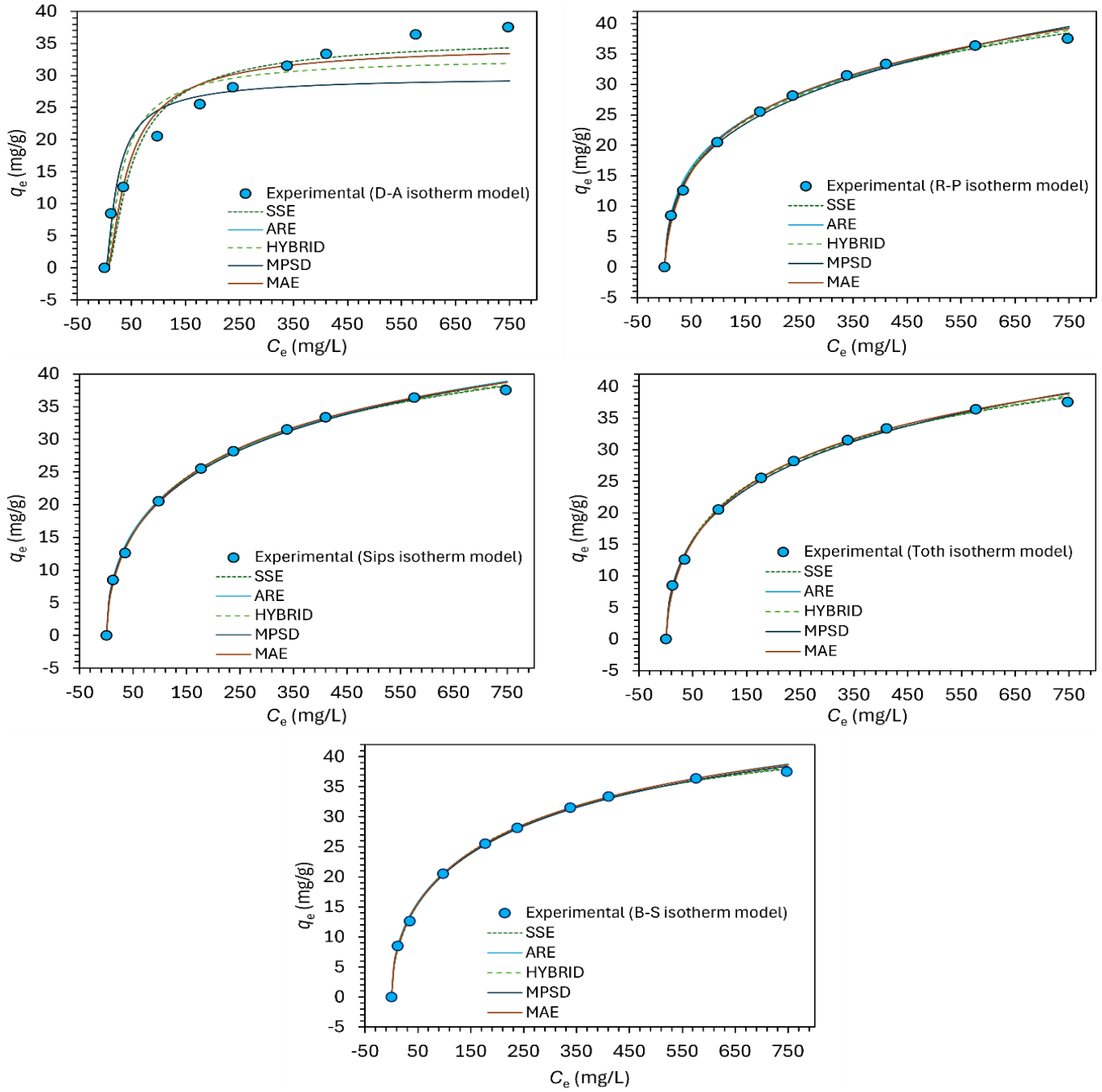

Figure 5. Comparison of experimental and model-predicted adsorption isotherm data using five different error functions (SSE, ARE, HYBRID, MPSD, and MAE) in Excel Solver for three-parameter isotherm models

Table 5. SNE values of the error functions for each isotherm model

	SNE values of the error functions				
Isotherm models	**SSE**	**ARE**	**HYBRID**	**MPSD**	**MAE**
Two-parameter isotherms					
Langmuir	3.70984	3.61598	**3.61199**	4.53198	3.93875
Freundlich	4.05970	4.28821	**3.66474**	3.78812	4.40430
Temkin	**3.16987**	3.70161	3.19093	3.74981	4.60252
Dubinin-Radushkevich (D-R)	4.82714	**4.72253**	4.77686	4.89615	**4.72253**
Jovanovic	4.02794	**3.86097**	3.91426	4.72459	4.09582
Three-parameter isotherms					
Dubinin-Astakhov (D-A)	4.11272	**3.83680**	3.96452	4.63291	3.83680
Redlich-Peterson (R-P)	3.93307	3.90563	**3.70067**	4.29188	4.37635
Sips	4.06653	4.38250	**3.84006**	4.45807	4.19596
Tóth	3.97924	4.21515	**3.79232**	4.42643	4.37074
Brouers–Sotolongo (B-S)	3.83243	4.42005	**3.65970**	4.26676	3.93762

Fig. 8 collectively illustrates the C_e–q_e plots drawn for each model based on the error functions with the lowest SNE values. Fig. 9 provides this representation individually. From these graphs, the model that best represents (or describes/explains) the experimental data can be selected.

When examining Fig. 8, and especially Fig. 9 and Fig. 10, it becomes evident that the isotherms that least represent the experimental data are D-R and D-A. Except for D-A, all three-parameter isotherms represent the experimental data very well. In Fig. 8 and Fig. 10, distinguishing between the R-P, Sips, Toth, and B-S isotherms is particularly challenging. All these isotherms were best minimized using the HYBRID error function. Therefore, a ranking among the models can be made using the HYBRID error function values in Table 4. According to this, the ranking for best representation of the experimental data is as follows: B-S > Sips > Toth > R-P.

These four isotherms are followed by Freundlich > Temkin > Langmuir > Jovanovic > D-A > D-R. From these results, it can be concluded that D-A and D-R fail to represent the experimental data, whereas the others represent it to some extent. Let us now analyze the isotherms that best represent the experimental data in order.

In this study, the Brouers–Sotolongo (B-S) isotherm model undoubtedly provides the best representation of Pb^{2+} adsorption onto pine bark from aqueous solutions. The B-S parameters (constants) determined in this study are K_{BS} = 0.05101 and α_{BS} = 0.52976. The K_{BS} value indicates that the binding energy between the adsorbent and adsorbate is low to moderate. This suggests that the adsorption process does not require high binding energy and that the energy levels of the adsorption sites on the surface are limited. The α_{BS} parameter typically ranges between 0 and 1. An α_{BS} value of approximately 0.5 reflects a heterogeneous surface structure, indicating that the adsorption sites on the surface exhibit varying energy levels. The B-S isotherm can be considered a hybrid model, essentially an adaptation of the Langmuir isotherm for heterogeneous surfaces. The perfect fit of the experimental data to this model indicates that the material possesses a structure that combines both homogeneous and heterogeneous surface characteristics.

The experimental data also show excellent compatibility with other three-parameter isotherms, such as the R-P, Sips, and Tóth models, similar to the B-S model. Three-parameter isotherm models are designed to describe more complex adsorption mechanisms that two-parameter models, like Langmuir and Freundlich, fail to explain adequately. The compatibility of the data with these models suggests that the adsorption process involves a more intricate nature, encompassing both homogeneous and heterogeneous surface characteristics with diverse energetic and structural features.

The Tóth isotherm is an empirical extension of the Langmuir model; however, by incorporating the dimensionless parameter n_T in its mathematical expression, it accounts for surface heterogeneity, which is neglected in the Langmuir model. As will be evident from the results obtained in this study, this adjustment enhances its fit with experimental data. In Table 4, the n_T parameter for the Tóth isotherm is approximately 0.30 (as determined by HYBRID minimization). The fact that $n_T < 1$ indicates that the adsorbent surface possesses a relatively heterogeneous structure.

A similar approach can also be applied to the Sips isotherm, which presents a hybrid model by combining the characteristics of both the Langmuir and Freundlich isotherms. The critical parameter in this model is β_S. In this study, the calculated β_S value is approximately 0.57 (Table 4). The dimensionless heterogeneity parameter β_S reflects surface homogeneity and the degree of deviation in adsorption. A $\beta_S < 1$ value indicates that the adsorbent surface is heterogeneous and contains adsorption regions with varying energy levels.

Another isotherm model with a similar approach and mathematical expression is the Redlich-Peterson (R-P) model. The mathematical expression of the R-P model is given in Eq. (16), where the parameter β_{RP} takes values between 0 and 1. As β_{RP} approaches 1, the model reduces to the Langmuir isotherm, while as β_{RP} approaches 0, it resembles the Freundlich isotherm. The values of β_{RP} between 0 and 1 characterize the heterogeneity of the adsorbent surface. In this study, β_{RP} is approximately 0.75 (Table 4). Consequently, most of the three-parameter isotherms share similarities with one another.

In this study, the models that least represent the experimental data, or perhaps do not represent them at all, are primarily the two-parameter Dubinin-Radushkevich (D-R) isotherm, followed by the three-parameter Dubinin-Astakhov (D-A) isotherm. The D-R isotherm is more suitable for describing adsorption behavior occurring on microporous, homogeneous surfaces with uniform adsorption energies. However, the pine bark used in this study was employed in its original, untreated form, characterized by a limited pore structure, low surface area, and heterogeneous surface properties. Therefore, it is unsurprising that the adsorption of Pb^{2+} does not fit this model.

The D-A model, another isotherm model that struggles to represent experimental data, is actually an extended version of the D-R model. In the D-A model, the n_{DA} parameter (Eq. (15)) ensures that the model has three parameters, providing information about the heterogeneity of the adsorbent and allowing its

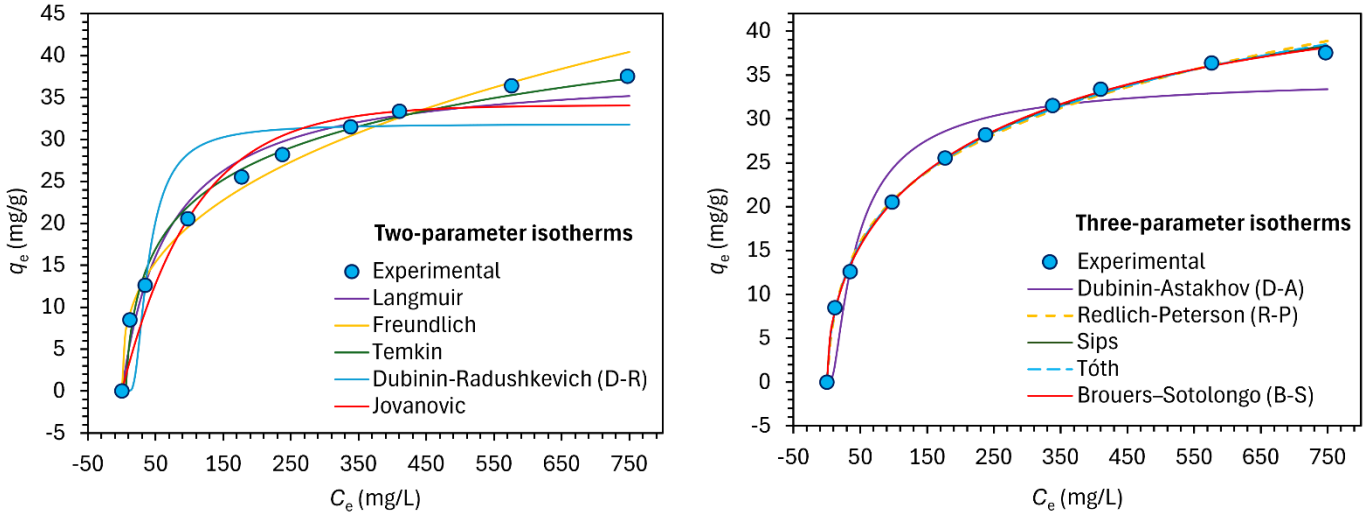

Figure 6. Comparison of two- and three-parameter isotherms optimized in Excel Solver

application to adsorbents on heterogeneous surfaces. The E constant in Eq. (15) characterizes the adsorption energy. When the E value is below 8 kJ/mol, adsorption generally proceeds through physical interactions. In this study, it is observed from Table 4 that the E value is 2.37 kJ/mol (determined by ARE minimization). In Table 4, the n_A values for this model are exactly 1. The n_A = 1 condition indicates that adsorption occurs on homogeneous surfaces. However, other isotherms suggest that the adsorbent surface is more heterogeneous. Since experimental data do not strongly support the D-A model, it may be more appropriate to disregard this result.

Among the commonly used two-parameter isotherms, the Langmuir and Freundlich models are the most well-known. The Langmuir isotherm, which is highly successful in describing monolayer adsorption processes on homogeneous surfaces, fails to fully describe the adsorption of Pb^{2+} onto red pine bark, which is determined to have a heterogeneous structure, as shown in Fig. 8 and Fig. 9. Specifically, experimental data deviate from the Langmuir model beyond the inflection point of the curve, as observed in Fig. 9.

On heterogeneous surfaces, the presence of regions with varying energy levels causes a delay in reaching equilibrium after the inflection point of the adsorption curve. In contrast, the Langmuir model assumes that the adsorption sites on the surface have uniform energy, resulting in a rapid attainment of equilibrium and the formation of a flat plateau beyond the inflection point. This behavior highlights the limitations of the Langmuir isotherm in describing adsorption on heterogeneous surfaces.

On the other hand, as evidenced by Fig. 8 and particularly Fig. 9, the experimental data are better represented by the Freundlich isotherm. This observation is further supported by the data presented in Table 3. The coefficient of determination (R^2) values, which indicate the degree of fit between the models and the experimental data, are R^2 = 0.98047 for the Langmuir model and R^2 = 0.98910 for the Freundlich model. These results demonstrate that the Freundlich isotherm provides a more accurate representation of adsorption processes on heterogeneous surfaces.

Compared to these two well-known models, it is observed that the Temkin isotherm better represents the experimental data (Fig. 9). The R^2 value for the Temkin isotherm is 0.99150 (Table 3). As noted in **Section 3.2.1**, the Temkin isotherm accounts for the non-uniform energy distribution on the adsorbent surface. Therefore, the high degree of representation of the data by the Temkin isotherm is a reasonable outcome.

The Jovanovic isotherm is the third least representative model for the experimental data. In Table 3, the Jovanovic parameters are reported as K_J = 0.00944 L/mg, $q_m \approx 34$ mg/g, and R^2 = 0.96662. These results indicate that the Jovanovic model weakly explains the adsorption process in the system. Similar to the Langmuir model, the Jovanovic isotherm focuses on homogeneous surfaces and monolayer adsorption processes. Therefore, such a result is not surprising.

5. Conclusions

This study provides a comprehensive evaluation of Pb^{2+} ion adsorption onto pine bark, emphasizing the use of advanced modeling and error analysis techniques to enhance the reliability of kinetic and equilibrium data interpretation. Key findings are as follows:

Pine bark demonstrated moderate to high adsorption capacity, making it a viable, low-cost material for heavy metal removal from aqueous solutions.

The Brouers-Sotolongo (B-S) kinetic model best described the adsorption kinetics, indicating a mixed mechanism involving both physical and chemical interactions. The half-reaction time ($\tau_{1/2}$ = 10.99 min) and fractal time parameter (α_{BS} = 0.64329) highlighted the system's heterogeneity.

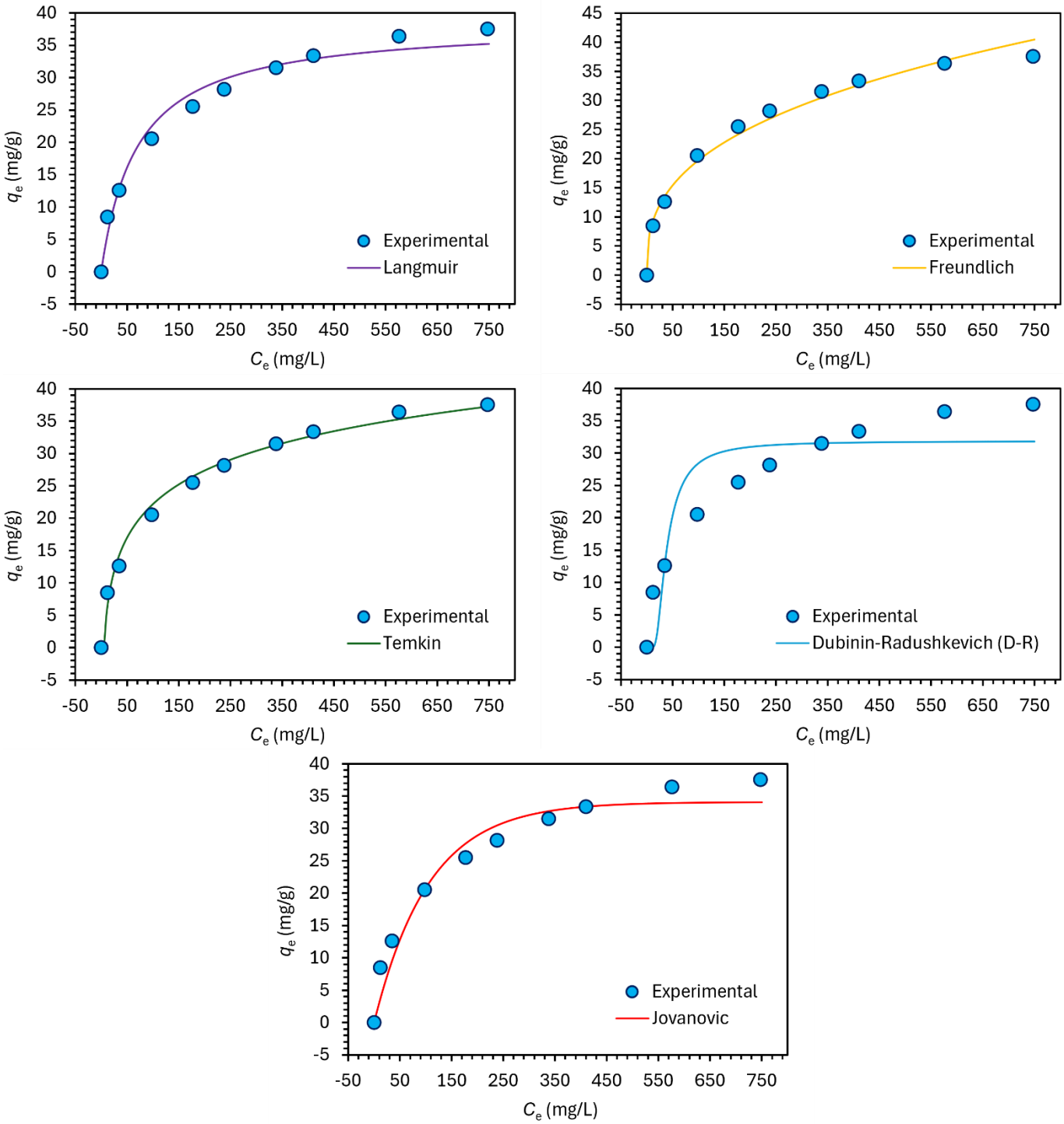

Figure 7. Single representations of two-parameter isotherms optimized in Excel Solver

Three-parameter isotherms, particularly the B-S, Tóth, and Sips models, provided the most accurate representation of experimental data. These models effectively captured the complexity of the adsorption process, including surface heterogeneity and variable energy distributions.

Non-linear regression using Microsoft Excel Solver proved to be an accessible and effective tool for optimizing adsorption model parameters. The HYBRID error function was identified as the most robust method for evaluating model performance.

The results reinforce the potential of using pine bark as an environmentally friendly adsorbent in wastewater treatment applications. Furthermore, this study highlights the importance of selecting appropriate models and error functions to ensure accurate data interpretation, particularly for systems with complex adsorption mechanisms.

In conclusion, this research contributes to the understanding of Pb^{2+} adsorption processes and demonstrates the practical application of advanced modeling techniques in environmental remediation studies. This study also contributes to the literature by

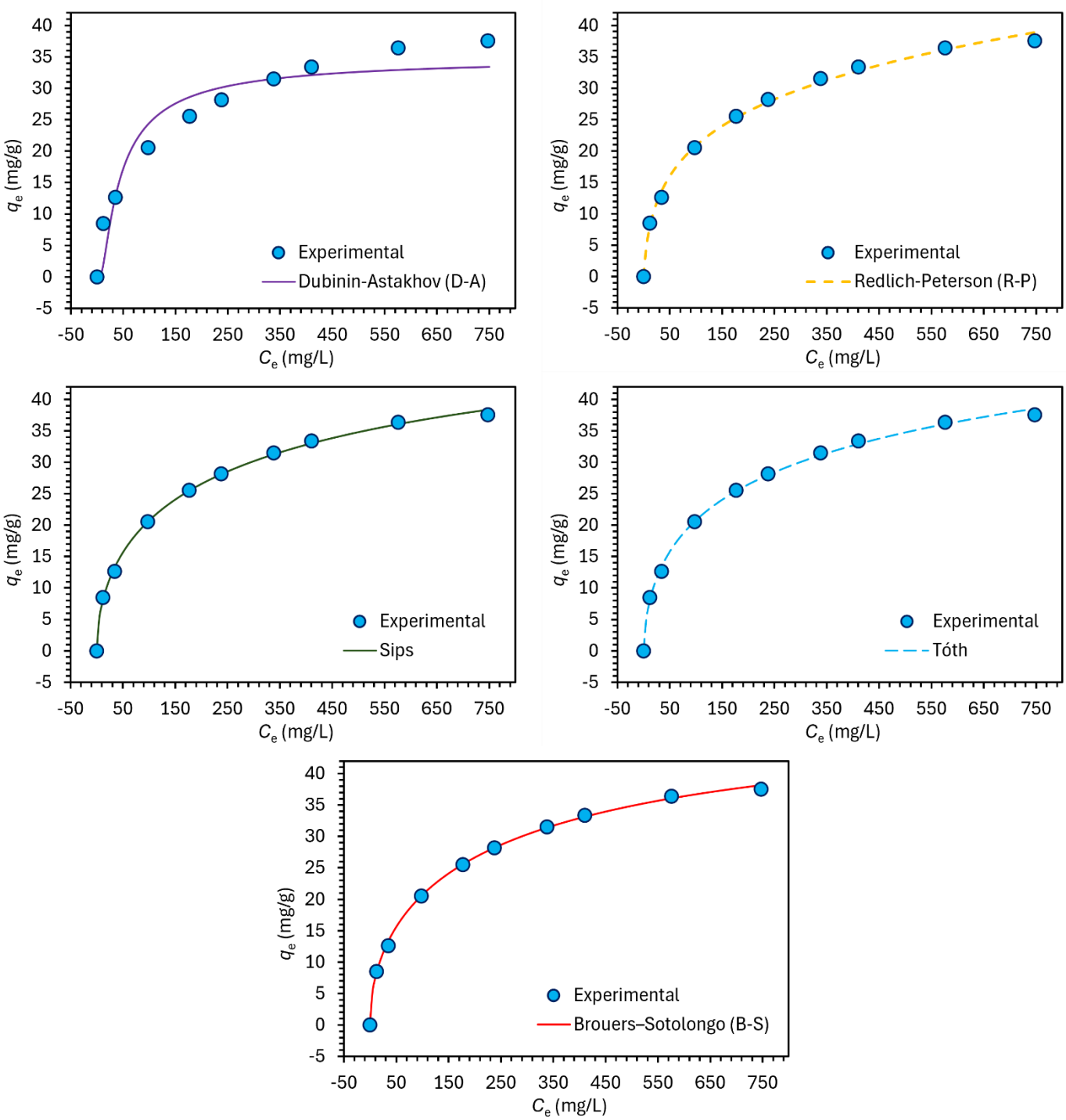

Figure 8. Single representations of three-parameter isotherms optimized in Excel Solver

demonstrating how the minimization of error functions using Microsoft Excel Solver enables more accurate interpretation and representation of equilibrium and kinetic data. This approach facilitates the selection of purpose-specific adsorbents and provides a deeper understanding of adsorption mechanisms. In addition, it is suggested that the selected method in this study can help eliminate the complexities and confusions found in the literature regarding this topic. It has been concluded that using Excel Solver with a non-linear approach allows for more accurate processing of adsorption data and better reflects the adsorption mechanism of the selected adsorbent.

References

[1] A.M. Badran, U. Utra, N.S. Yussof, M.J.K. Bashir, Advancements in adsorption techniques for sustainable water purification: A focus on lead removal, Separations 10(11), 2023, 565.

[2] N.e. Hira, S.S.M. Lock, N.F. Shoparwe, I.S.M Lock, L.G. Lim, C.L. Yiin, Y.H. Chan, M. Hassam, Review of Adsorption Studies for Contaminant Removal from Wastewater Using Molecular Simulation, Sustainability, 15(2), 2023, 1510.

[3] U.A. Edet, A.O. Ifelebuegu, Kinetics, isotherms, and thermodynamic modeling of the adsorption of phosphates from model wastewater using recycled brick waste, Processes, 8(6), 2020, 665.

[4] K.Y. Foo, B.H. Hameed, Insights into the modeling of adsorption isotherm systems, Chem Eng J, 156(1), 2010, 2–10.

[5] H.R. Ghaffari, H. Pasalari, A. Tajvar, K. Dindarloo, B. Goudarzi, V. Alipour, A. Ghanbarneajd, Linear and nonlinear two-parameter adsorption isotherm modeling: A case-study, Int J Eng Sci, 6(9), 2017, 1–11.
[6] L.S. Chan, W.H. Cheung, S.J. Allen, G. McKay, Error analysis of adsorption isotherm models for acid dyes onto bamboo derived activated carbon, Chinese J Chem Eng, 20(3), 2012, 535–542.
[7] K. Suwannahong, S. Wongcharee, T. Kreetachart, C. Sirilamduan, J. Rioyo, A. Wongphat, Evaluation of the Microsoft Excel Solver spreadsheet-based program for nonlinear expressions of adsorption isotherm models onto magnetic nanosorbent, Appl Sci, 11(16), 2021, 7432.
[8] E.A. Adekunbi, J.O. Babajide, H.O. Oloyede, J.S. Amoko, O.A. Obijole, I.A. Oke, Evaluation of Microsoft Excel Solver as a tool for adsorption kinetics determination, Ife J Sci, 21(3), 2019, 169–183.
[9] J. Sreńscek-Nazzal, U. Narkiewicz, A.W. Morawski, R.J. Wróbel, B. Michalkiewicz, Comparison of optimized isotherm models and error functions for carbon dioxide adsorption on activated carbon, J Chem Eng Data, 60(11), 2015, 3148–3158.
[10] Md A. Hossain, H.H. Ngo, W. Guo, Introductory of Microsoft Excel Solver function – spreadsheet method for isotherm and kinetics modelling of metals biosorption in water and wastewater, J Water Sustain, 3(4), 2013, 223–237.
[11] Y.S. Ho, G. McKay, Sorption of dye from aqueous solution by peat, Chem Eng J, 70(2), 1998, 115–124.
[12] Sahmoune Mohamed Nasser, Moussa Abbas, Mohamed Trari, Understanding the rate-limiting step adsorption kinetics onto biomaterials for mechanism adsorption control, Prog React Kinet Mec, 49, 2024, 1–26.
[13] B. Mehdinejadiani, S.M. Amininasab, L. Manhooei, Linear and non-linear methods for estimating isotherm parameters of nitrate adsorption, Water resources and wetlands, 4th International Conference Water resources and wetlands, 5-9 September 2018, Tulcea (Romania), p.312.
[14] G.W. Kajjumba, S. Emik, A. Öngen, H.K. Özcan, S. Aydın, Modelling of Adsorption Kinetic Processes—Errors, Theory and Application. In Advanced Sorption Process Applications. Edited by Serpil Edebali, Published: 05 November 2018, IntechOpen.
[15] J.-C. Liu, P. A. Monson, Monte Carlo simulation study of water adsorption in activated carbon, Ind Eng Chem Res, 45(16), 2006, 5649–5656.
[16] A. Wongphat, S. Wongcharee, N. Chaiduangsri, K. Suwannahong, T. Kreetachat, S. Imman, N. Suriyachai, S. Hongthong, P. Phadee, P. Thanarat, J. Rioyo, Using Excel Solver's parameter function in predicting and interpretation for kinetic adsorption model via batch sorption: Selection and statistical analysis for basic dye removal onto a novel magnetic nanosorbent, Chem Eng, 8(3), 2024, 58.
[17] A. Gundogdu, D. Ozdes, C. Duran, V.N. Bulut, M. Soylak, H.B. Senturk, Biosorption of Pb(II) ions from aqueous solution by pine bark (*Pinus brutia* Ten.) Chem Eng J, 153(1-3), 2009, 62–69.
[18] S. Lagergren, About the theory of so-called adsorption of soluble substances. Kungliga Svenska Vetenskapsakademiens Handlingar, 24(4), 1898, 1–39.
[19] Y.S. Ho, Review of second-order models for adsorption systems. J Hazard Mater, 136(3), 2006, 681–689.
[20] L. Largitte, R. Pasquier, A review of the kinetics adsorption models and their application to the adsorption of lead by an activated carbon, Chem Eng Res Design, 109, 2016, 495–504,
[21] M. Avrami, Kinetics of phase change. I. General theory. J Chem Phys, 7(12), 1939, 1103–1112.
[22] R. George, S. Sugunan, Kinetics of adsorption of lipase onto different mesoporous materials: Evaluation of Avrami model and leaching studies, J Mol Catal B-Enzymatic, 2014, 105, 26–32.
[23] A.G. Marangoni, Kinetics of crystal growth using the Avrami model and the chemical potential approach. In: Kinetic analysis of food systems, 2017, Springer, Cham.
[24] F. Brouers, The fractal (BSf) kinetics equation and its approximations. J Mod Phys, 5(16), 2014, 1594–1601.
[25] F. Brouers, T.J. Al-Musawi, The use of the Brouers–Sotolongo fractal kinetic equation for the study of drug release. Adsorption 26, 2020, 843–853.
[26] S. Karoui, R.B. Arfi1, M.J. Fernández-Sanjurjo, A. Nuñez-Delgado, A. Ghorbal1, E. Álvarez-Rodríguez, Optimization of synergistic biosorption of oxytetracycline and cadmium from binary mixtures on reed-based beads: modeling study using Brouers-Sotolongo models, Environ Sci Pollut R, 28, 2021,46431–46447.
[27] A.M.B. Hamissa, F. Brouers, M.C. Ncibi, M. Seffen, Kinetic modeling study on methylene blue sorption onto agave americana fibers: Fractal kinetics and regeneration studies, Sep Sci Technol, 48(18), 2013, 2834-2842,
[28] I. Langmuir, The adsorption of gases on plane surfaces of glass, mica, and platinum, J Am Chem Soc, 40(9), 1918, 1361–1403.
[29] A. Saha, D. Bhaduri, A. Pipariya, R.K. Ghosh, Linear and nonlinear sorption modelling for adsorption of atrazine onto activated peanut husk, Environ Prog Sustain, 36(2), 2017, 348–358.
[30] H. Freundlich, Over the adsorption in solution. Journal of Physical Chemistry, 57, 1906, 385–471.
[31] M.J. Temkin and V. Pyzhev, Recent modifications to Langmuir isotherms, Acta Physiochim. USSR, 12 (1940) 217–222.
[32] M.M. Majd, V. Kordzadeh-Kermani, V. Ghalandari, A. Askari, M. Sillanpää, Adsorption isotherm models: A comprehensive and systematic review (2010–2020), Sci Tot Environ, 812, 2022, 151334.
[33] N.D. Hutson, R.T. Yang, Theoretical basis for the Dubinin-Radushkevitch (D-R) adsorption isotherm equation, Adsorption, 3, 1997, 189-195.
[34] R. Saadi, Z. Saadi, R. Fazaeli, N.E. Fard, Monolayer and multilayer adsorption isotherm models for sorption from aqueous media, Korean J. Chem. Eng., 32(5), 2015, 787–799.
[35] M.M. Dubinin, V.A. Astakhov, Development of the concepts of volume filling of micropores in the adsorption of gases and vapors by microporous adsorbents, Russ Chem Bull, 20, 1971, 3–7.
[36] G.J. Millar, S.J. Couperthwaite, M. de Bruyn, C.W. Leung, Ion exchange treatment of saline solutions using Lanxess S108H strong acid cation resin, Chem Eng J, 280, 2015, 525–535.
[37] V.J. Inglezakis, Solubility-normalized Dubinin–Astakhov adsorption isotherm for ion-exchange systems, Micropor Mesopor Mat, 103(1-3), 2007, 72–81.
[38] O. Redlich, D.L. Peterson, A useful adsorption isotherm, J Phys Chem, 63(6), 1959, 1024–1024.
[39] S. Kalam, S.A. Abu-Khamsin, M.S. Kamal, S. Patil, Surfactant adsorption isotherms: A review, ACS Omega, 6(48), 2021, 32342–32348,
[40] J. Toth, State equations of the solid gas interface layer, Acta Chem Acad Hung, 69 (1971) 311–317.
[41] L Bokányi, Some applications of Tóth-isotherm in mineral processing, XXVI International Mineral Processing Congress (IMPC) 2012 Proceedings, New Delhi, India, 24–28 September 2012.
[42] R. Ramadoss, D. Subramaniam, Removal of divalent nickel from aqueous solution using blue-green marine algae: adsorption modeling and applicability of various isotherm models, Sep Sci Technol, 54(6), 2019, 943–961.
[43] F. Brouers, O. Sotolongo, F. Marquez, J.P. Pirard, Microporous and heterogeneous surface adsorption isotherms arising from Levy distributions. Physica A, 349(1-2), 2005, 271–282.
[44] F. Gimbert, N. Morin-Crini, F. Renault, P.-M. Badot, G. Crini, Adsorption isotherm models for dye removal by cationized starch-based material in a single component system: Error analysis, J Hazard Mater, 157(1), 2008, 34–46.

[45] N. Sivarajasekar, R. Baskar, Adsorption of Basic Magenta II onto H_2SO_4 activated immature Gossypium hirsutum seeds: Kinetics, isotherms, mass transfer, thermodynamics and process design, Arab J Chem, 12(7), 2019, 1322–1337.
[46] C.J. Willmott, K. Matsuura, Advantages of the mean absolute error (MAE) over the root mean square error (RMSE) in assessing average model performance, Clim Res, 30, 2005, 79–82.
[47] N.R. Draper, H. Smith, Applied Regression Analysis. 3th Edition, 1998, Wiley, New York.
[48] R.J. Hyndman, A.B. Koehler, Another look at measures of forecast accuracy, Int J Forecasting, 22(4), 2006, 679–688.
[49] W.H. Press, S.A. Teukolsky, W.T. Vetterling, B.P. Flannery, Numerical recipes: The art of scientific computing (3rd ed.), 2007, Cambridge University Press.